PHOTOCATALYTIC REDUCTION OF CARBON DIOXIDE IN CONJUNCTION WITH DECOMPOSITION OF WATER ON OXIDE SEMICONDUCTOR SURFACES

A project Report

Submitted in partial fulfilment of the requirements

For the award of the degree of

MASTER OF TECHNOLOGY

In

CHEMICAL ENGINEERING

SPECIALISATION : CATALYSIS TECHNOLOGY

By

K. RAJALAKSHMI

(CH09M003)

Under the guidance of

Dr. K.R.Krishnamurthy

Dr.R.Ramnarayanan

DEPARTMENT OF CHEMICAL ENGINEERING

INDIAN INSTITUTE OF TECHNOLOGY, MADRAS

CHENNAI – 600 036

MAY, 2011

CERTIFICATE

This is certify that the project report entitled "**PHOTOCATALYTIC REDUCTION OF CARBON DIOXIDE IN CONJUNCTION WITH DECOMPOSITION OF WATER ON OXIDE SEMICONDUCTOR SURFACES "** submitted by **K.Rajalakshmi** (**CH09M003**) to the Indian Institute of Technology, Madras for the award of the degree of Master of technology in Catalysis Technology, Chemical Engineering is a bonafide record of the work carried out by her under my supervision. The contents of the thesis, in full or parts have not been submitted to any other institute or university for the awards of any degree **.**

Research Guides

Dr. K.R. Krishnamurthy
National Centre for Catalysis Research
IIT Madras.

Dr. R. Ramnarayanan
Department of Chemical Engineering
IIT Madras

Chennai – 600 036

Date:

ACKNOWLEDGEMENTS

I am deeply indebted to my research guides **Dr. K.R.Krishnamurthy** and **Prof. R.Ramnarayanan** for their incessant encouragement, thought provoking discussions and unfailing guidance at every stage of the research programme. It gives me immense pleasure to have been associated with them. It is my privilege to express my gratitude tothem for introducing me to the field of catalysis. I thank them for their patient guidance,open discussions, constant encouragement, unbounded enthusiasm and interest and I owe them a great intellectual and inspirational debt.

I express my sincere gratitude to **Prof. B. Viswanathan** for his inspiring, invaluable guidance, constant encouragement and thought provoking discussions through out the research work. I am really grateful to him for providing opportunities to learn various aspects in catalysis. I feel privileged to have been associated with him.

I express my deep gratitude to **Dr.S.Pushpavanam**, Head,Department of Chemical Engineering for the support and facilities provided in carrying out this project work.I would like to thank the M.Tech project evaluation committee **Dr.S.Sivasankar,Prof P.Selvam** and **Prof Preeti Agalyam** for their useful comments and suggestions. I am great full to **NCCR** for providing me all the facilities through out my project.
I thank the **Head and staff members of CGBS, SAIF** and **Department of Metallurgy** IIT Madras for providing the necessary instrumentation facilities.I am thankful to **Prof Ravi krishna** for his timely guidance in product analysis.

I express my heart full thanks to **V. Jeyalakshmi** for her constant help and support which made it possible for me to complete my work. I am thankful to my classmates **Devaki**,**Chaitanya**, **Sourav** and **Sanjay** for their instant help and support.
I thank my senior colleagues **Mr. Kuppan, Mr. Vamsi, Mr. Ramana, Mr. Mahendran, Mr.Muthukrishnan, Mr.Sankaranarayanan, Ms. Alagarasi, Ms.Keerthiga, Mr. Suthagar, Ms. Banu, Dr. Thirunavukkarasu, Ms. Deepa, Ms. Vijayashanti ,Mr.Rammohan ,Mr. Pachamuthu, Mr. Prakash, Ms.Kavya,Mr.Shanmugam** for their help in all aspects.

Last but not least I owe everything to **my parents** , **grand parents** and **sister** for their constant support and encouragement whenever needed, without them it would have been impossible for me to complete this work.

K.Rajalakshmi

ABSTRACT

KEY WORDS: Photocatalysis, CO_2 reduction, TiO_2, water splitting, layered perovskite,band gap.

Carbon dioxide accounts for the largest share of the world's greenhouse gas emissions. There is a growing need to mitigate CO_2 emissions. Some of the strategies to mitigate CO_2 emissions are energy conservation, carbon capture and storage and using CO_2 as a raw material in chemical processes. Reactions involving CO_2 typically require energy input and/or a high energy substrate. The energy source should be provided without producing more CO_2, such as solar energy. One of the best routes to remedy CO_2 is to transform it to hydrocarbons via photo reduction. There by, solar energy is transformed and stored as chemical energy. The most ideal and desirable process would then be the simultaneous reduction of CO_2 and water to yield hydrocarbons, which essentially works out to artificial photosynthesis.

Among various semiconductors, TiO_2 is widely used in many photoinduced processes because of its comparatively low cost, low toxicity and its ability to resist photocorrosion. The effect of transition metal ion on TiO_2 was studied for CO_2 photoreduction. Addition of noble metal to TiO_2 can change the distribution of electrons and they prevent the electron hole recombination, thereby enhancing the Photocatalytic efficiency of TiO_2.Also the effect of coupling TiO_2 with other metal oxide semiconductors (CuO,NiO) for CO_2 photoreduction was studied.

Wide band gap semiconductor materials are the most suitable for CO_2 photoreduction. Since water is used as the reductant, the catalyst should be capable of splitting water into hydrogen and oxygen. NiO/La:$NaTaO_3$ showed high activity for water splitting and quantum efficiency of 56% was observed for this catalyst. Hence NiO/La:$NaTaO_3$ was tested for CO_2 photoreduction with water. Layered pervoskite such as $Sr_3Ti_2O_7$ and NiO/Ba:$La_2Ti_2O_7$ which was active towards water splitting were also tested for CO_2 photoreduction.

TABLE OF CONTENTS

Table of contents (Contd.,) **Page No.**

Table of contents (Contd.,) **Page No.**

Table of contents (Contd.,) **Page No.**

LIST OF TABLES

LIST OF FIGURES

LIST OF SCHEMES

ABBREVIATIONS

AR	-	Analytical Reagent
GC	-	Gas Chromatography
FID	-	Flame Ionisation Detector
SEM	-	Scanning electron microscopy
EDS	-	Energy Dispersive Spectra
TPR	-	Temperature Programmed Reduction
TEM	-	Transmission Electron Microscopic
UV-Vis	-	Ultraviolet-Visible
XRD	-	X-ray Diffraction
LUMO	-	Lowest Unoccupied Molecular Orbital
HOMO	-	Higher Occupied Molecular Orbital
NHE	-	Normal Hydrogen Electrode
E_{cb}	-	Conduction Band Energy
E_{vb}	-	Valence Band Energy
ppm	-	parts per million
E_g	-	Band gap energy

NOTATIONS

eV	- electron volt
m^2/g	- Square meter per gram
°C	- degree celsius
g	- gram
h	- hour
nm	- nano meter
Å	- Angstrom
λ	- Wavelength
wt	- Weight
θ	- Bragg's angle
μmol	- micro mol
ν	- frequency
d	- Interplanar spacing
Gt	- Giga ton
W	- Watt
e^-	- electron
h^+	- hole
Φ	- Work function.

CHAPTER 1

INTRODUCTION

1.1 HETEROGENEOUS PHOTO CATALYSIS

The study of photo catalytic reactions was initiated in 1970's. The concept and the term ''heterogeneous photo catalysis'' were introduced and developed in Lyon to describe the partial oxidation of alkanes and olefinic hydrocarbons .The reactions took place at ambient temperature in the presence of titanium dioxide (TiO_2, anatase) under UV irradiation.

Heterogeneous photocatalysis is defined by Palmisano and Sclafani (1997) as "a catalytic process during which one or more reaction steps occur by means of electron–hole pairs photo generated on the surface of semiconducting materials illuminated by light of suitable energy." This pathway differs from the usual thermal reaction sequence and leads to reaction product selectivities different from those for the thermal/ catalyzed reactions.

1.2 PRINCIPLES AND ELEMENTARY STEPS

The band gap is characteristic for the electronic structure of a semiconductor and is defined as the energy interval (ΔE_g) between the valence band (VB) and the conduction band (CB). VB is defined as the highest energy band in which all energy levels are occupied by electrons, whereas CB is the lowest energy band without electrons.

According to the band gap model (Demeestere *et al*.,2007) as shown in fig 1.1, VB electrons are transferred to the CB when the semiconductor is illuminated with photons having an energy content equal to or higher than the band gap, creating electron–hole pairs (1). After migration to the semiconductor surface (2), electron–hole pairs may induce redox reactions with adsorbates having suitable redox potentials (3). From a thermodynamic point of view, VB holes can oxidize adsorbed compounds if the redox potential of the VB is more positive than that of the adsorbates. Similarly, CB electrons can reduce adsorbed species if they have a more negative redox potential than the adsorbates . In the absence of suitable adsorbates, electron–hole pair recombination occurs with release of thermal energy and/or light (4).

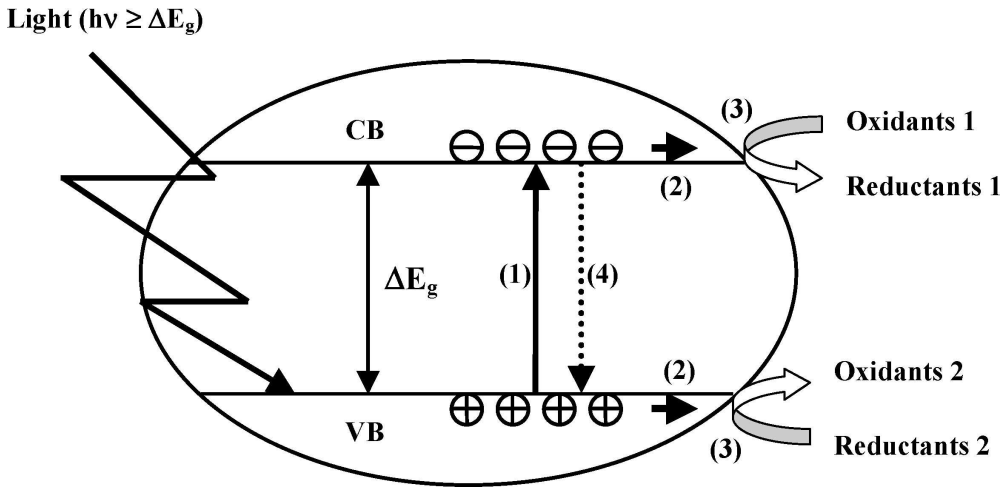

Scheme 1.1 Schematic representation of the "band gap model." (1) Photo induced electron– hole pair creation; (2) charge migration to the surface; (3) redox reactions; (4) recombination. VB and CB represent valence band and conduction band, respectively.

The rate of a photo catalytic reaction especially depends on the type of the photo catalytic semiconductor and on the light radiation that it used in its initiation (Koci *et al*.,2008). Further factors that influence a photo catalytic reaction are:

– pH of the medium with which the semiconductor surface is in contact;
– concentration of the substrate influencing the reaction kinetics;
– stream of photons, as oversupply of light accelerates electron–hole recombination;
– temperature, higher temperatures cause frequent collision between the semiconductor and the substrate

1.3 APPLICATIONS

A variety of applications ranging from anti□fogging, anti□microbial and self□cleaning surfaces, through to water and air purification and solar induced hydrogen production, have been developed and many of these have made their way into commercial products. However, extensive research continues to further optimise this technology and to widen the spectrum of potential applications, especially in the following areas namely,

- Conversion of water to hydrogen gas by photo catalytic water splitting. The ultimate target of water splitting is to provide clean H_2 fuel through the utilization of solar energy. Considerable efficiencies for solar water splitting have been reported for the photovoltaic–photoelectrolytic device of Khaselev and Turner and for the photovoltaic–electrolytic device of Licht (Fujishma *et al*., 2006).
- Conversion of carbon dioxide into hydrocarbons using water. In this case, Photo catalysis provides a way to mimic photosynthesis by employing a semiconductor catalyst to absorb and utilize solar energy to convert chemicals into other forms.
- The application of illuminated semiconductors for the remediation of contaminants has been used successfully for a wide variety of compound such as alkanes, aliphatic alcohols, aliphatic carboxylic acids, alkenes, phenols, aromatic carboxylic acids, dyes, PCB's, simple aromatics, halogenated alkanes and alkenes, surfactants, and pesticides as well as for the reductive deposition of heavy metals (e.g., Pt^{4+}, Au^{3+}, Rh^{3+}, Cr(VI)) from aqueous solution to surfaces (Hoffmann *et al*.,1995).
- Use of titanium dioxide in self-cleaning glass. Free radicals generated from TiO_2 oxidize organic matter .
- Photocatalytic surfaces have the potential to act against a variety of air pollutants and odours such as microbes, volatile organic carbons (VOC), formaldehyde, ammonia and inorganic gaseous substances such as nitrogen- or sulphur-oxides (NO_X, SO_X).
- Disinfection of water by titanium dioxide photo catalysis.

1.4 COMPONENTS OF A PHOTO CATALYST

In addition to the photo catalyst, whose primary function is to absorb light energy, several other components can be added to modify the photo catalyst system based on their application and improve overall efficiency (Stroyuk *et al*.,2009).

1.4.1 Photocatalytic system based on semiconductors and sensitizers

The large group of the light-sensitive materials that have been investigated as photo catalysts includes fairly wide-band semiconductors, mostly metal oxides, that absorb UV

light. One method of extending their light sensitivity to the visible region of the spectrum is the use of colored substances or sensitizers. In systems with sensitizers the dye absorbs visible light and in the excited state injects electrons into the semiconductor.

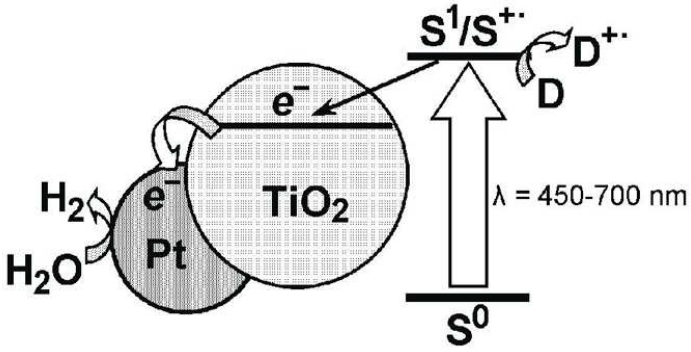

Scheme 1.2. Schematic diagram of the operation of the Photocatalytic system for the release of hydrogen from water based on metal–semiconductor structures and a dye–sensitizer. Legend: S^0, S^1, and $S^{+\cdot}$ are the sensitizer in the ground, excited, and one-electron oxidized states respectively .

1.4.2 Photo catalytic systems based on semiconductor hetero structures

In binary systems based on narrow-band and wide-band semiconductors the absorption of visible light by the narrow-band component also leads to the injection of an electron into the wide-band semiconductor. The hole remains spatially separated from the electron and interacts with the electron donor .

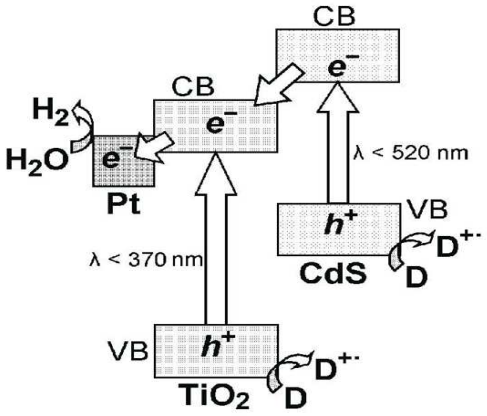

Scheme 1.3. Schematic diagram of the spatial separation of the photo generated charges in the CdS/TiO_2 hetero structure and the formation of hydrogen during the action of visible light .

1.4.3 Photo catalyst systems based on semiconductors doped with metal cations

The doping of wide-band semiconductors with transition metals creates local states in the forbidden band the excitation of which by visible light leads to the transfer of electrons into the conduction band.

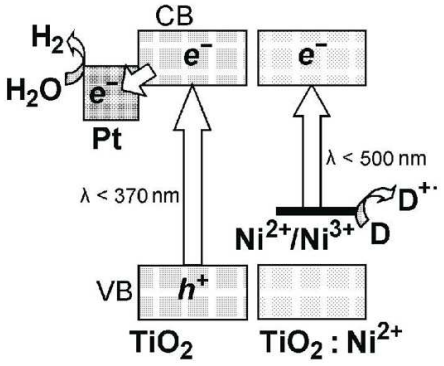

Scheme 1.4. Schematic diagram of the operation of the Photo catalytic system for the release of hydrogen from an aqueous solution of electron donor D with the participation of titanium dioxide doped with Ni^{2+} (TiO_2:Ni^{2+}) .

1.4.4 Photo catalyst systems based on semiconductors doped with anions

One of the approaches to narrowing of the forbidden band in oxide semiconductors was partial substitution of the oxygen by other elements (nitrogen, carbon, and sulfur), which makes it possible to realize “band design,” i.e., intentional shift of the valence band of the photocatalyst by virtue of the fact that the *p* orbitals of the impurity are situated in the valence band above the *p* orbitals of the oxygen, thereby narrowing the forbidden band without substantially moving the bottom of the conduction band .

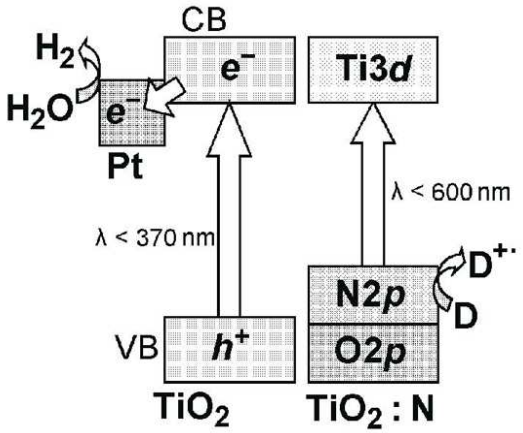

Scheme 1.5. Schematic diagram of the operation of the Photocatalytic system for the release of hydrogen from an aqueous solution of electron donor D with the participation of titanium dioxide doped with nitrogen (TiO_2:N) .

1.5 CO_2 MANAGEMENT- PHOTO CATALYSIS FOR CO_2 MITIGATION

CO_2 is a colorless and odorless gas. The molecule is linear with a double bond between the carbon and oxygen atoms (O= C=O). CO_2 occurs in nature and serves as source of carbon for photosynthesis of plants and crops. It is present in atmosphere with a volumetric concentration of 0.039 % (389 parts per million by volume, ppmv) .

The emission of carbon dioxide into the atmosphere, released mainly by the burning of fossil fuels is one of the most serious problems with regard to the greenhouse effect (Anpo,1995).All human activity generates about 37 billion tons (37 Gt) of CO_2 emissions each year, with about 30 Gt of this coming from energy-related emissions. Total emissions were less than 25 Gt twenty years ago, and under business as usual scenarios, emissions are projected to rise to over 50 Gt twenty years from now. Burning 1 t of carbon in fossil fuels releases more than 3.5 t of carbon dioxide (Maginn,2010). The Earth's surface temperature has risen by approximately 0.6 K in the past century, with particularly significant warming trends over the past two decades. Hence CO_2 reduction/management (capture, storage & sequestration) has become a key issue in controlling global warming.

1.6 REDUCTION OF CO_2 EMISSIONS

The reduction of CO_2 emissions can be achieved by three approaches (Usubharatana *et al*.,2006):

(1) Efficient use of carbon-based energy sources,

(2) Use of alternative or carbon-free energy sources,

(3) Use of a post treatment carbon-capture technology.

Carbon capture refers to the removal of CO_2 from industrial flue gas by a gas separation process prior to release to the atmosphere.

1.6.1 Sequestration

Carbon sequestration (storage) is the isolation of carbon dioxide (CO_2) from the earth's atmosphere. Sequestration can play a significant role in preventing continued CO_2 buildup in the atmosphere.

Geological sequestration involves storing CO_2 underground in rock formations that can retain large quantities of CO_2 for long periods of time. The CO_2 would be held in small pore spaces inherent in rocks. It is possible that CO_2 injection into coal seams and mature oil fields could assist in the extraction of coal bed methane or oil that would otherwise be left in the ground, which could help offset the costs of sequestration .

1.6.2 Other carbon capture technologies

Currently, technologies such as gas absorption into chemical solvents, permeation through membranes, cryogenic distillation, and gas adsorption onto a solid sorbent are available for the capture of CO_2 from flue gas. However these are not economically feasible (Usubharatana *et al* ,2006)

.

1.6.3 CO_2 conversion

CO_2 is the most oxidized form of carbon , and therefore the only chemical transformation

at normal energies that would be possible is to reduce it.

A wide range of CO_2 conversion techniques are under investigation (Aulice and Viswanathan ,2004) which include,

Chemical Reduction by metals which occur at relatively at high temperatures.

$$2Mg + CO_2 \rightarrow 2MgO + C \quad (1.1)$$

$$Sn + 2CO_2 \rightarrow SnO_2 + 2CO \quad (1.2)$$

$$2Na + 2CO_2 \rightarrow Na_2C_2O_4 \quad (1.3)$$

Thermochemical conversion

$$CO_2 \xrightarrow{Ce^{4+},T>900°C} CO + \frac{1}{2}O_2 \quad (1.4)$$

Radiochemical method

$$CO_2 \xrightarrow{\gamma-Radiation} HCOOH, HCHO \quad (1.5)$$

Photo-chemical conversion

$$CO_2 \xrightarrow{h\upsilon} CO, HCHO, HCOOH \quad (1.6)$$

Bio-chemical conversion

$$CO_2 + 4H_2 \xrightarrow{Bacteria} CH_4 + 2H_2O \quad (1.7)$$

The bacteria Methanobacterium thermoautotrophicum can be immobilized in a fixed bed or on hollow fibres, and feeding stoichiometric ratios for the reaction attains 80% of the theoretical yield.

electro-chemical conversion

$$CO_2 + xe^- + xH^+ \xrightarrow{eV} CO, HCOOH, (COOH)_2 \quad (1.8)$$

bio-photochemical conversion

The "bio" part of the energy consists in catalysis and information content of an enzyme.

$$CO_2 + \text{oxoglutaric acid} \xrightarrow{h\nu} \text{isocitric acid} \quad (1.9)$$

electro-photochemical conversion

$$CO_2 + 2e^- + 2H^+ \xrightarrow{h\nu,eV} CO + 2H_2O \quad (1.10)$$

Conventional catalytic reduction of CO_2 to chemicals (formic acid, methanol, methane etc.) with external hydrogen is feasible (Nam *et al*.,1999) but hydrogen has to be produced via renewable resources to render it viable and sustainable.

1.7 PHOTOCATALYTIC CO_2 REDUCTION

The CO_2 reduction process is thermodynamically uphill as illustrated by its standard free energy of formation ($\Delta G° = -394.359$ kJ/mol) (Indrakanti,2009). Economical CO_2 fixation is possible only if renewable energy, such as solar energy, is used as the energy source. Equally difficult is the reduction / splitting of water to yield hydrogen and hence requires similar combination of activation steps. The most ideal and desirable process would then be the simultaneous reduction of CO_2 and water to yield hydrocarbons, which essentially works out to artificial photosynthesis.

The utilization of solar energy via chemical storage can be achieved by photo catalytic or photo-electrochemical activation of light-sensitive catalytic surfaces. When comparing the two systems, photo catalytic system is simpler and easy to construct. Photocatalytic process occurs via the direct absorption of photons with energy greater than or equal to the band gap of the photo catalyst to generate electron-hole pairs. The initial excitation and electron energy transfer to the adsorbed reactants on the photo catalyst make chemical reactions in the photo catalytic process possible.

1.7.1 Thermodynamics

There are two conceptual routes to produce renewable carbon containing fuels using solar energy (Indrakanti,2009).

- The direct photo reduction of CO_2 using water as a reductant.
- The photolysis of water to generate hydrogen and further reaction of this hydrogen with carbon dioxide forming C_1–C_2 fuels.

Water and carbon dioxide splitting processes take place simultaneously on the photocatalyst/co-catalyst surface, and thermodynamic requirements of these processes put constraints on the band gap of the materials used as photocatalysts. Hydrogen formation from water involves a free energy change (ΔG^0) of 237 kJ/mol and an enthalpy change (ΔH^0) of 285 kJ/mol; the corresponding values for CO formation from CO_2 are 257 and 283 kJ/mol at 25°C (1 atm) (4). Hence, the minimum energy required for water and CO_2 splitting processes are, respectively, 1.229 and 1.33 eV (per photon). In theory, the band gap of a photocatalyst used for co-splitting of CO_2 and water should be at least 1.33 eV (Indrakanti,2009).

One, two, four, six and eight electron reduction potentials (vs. NHE) for CO_2 reduction and H_2O oxidation at pH 7 and 25°C assuming unit activities for all gaseous and aqueous species are given below (Indrakanti,2009)..

Reaction	E°_{redox}, V vs NHE
$2H^+ + 2e^- \rightarrow H_2$	-0.41
$H_2O \rightarrow \frac{1}{2}O_2 + 2H^+ + 2e^-$	0.82
$CO_2 + e^- \rightarrow CO_2^-$	-1.9
$CO_2 + H^+ + 2e^- \rightarrow HCO_2^-$	-0.49
$CO_2 + 2H^+ + 2e^- \rightarrow CO + H_2O$	-0.53
$CO_2 + 4H^+ + 4e^- \rightarrow HCHO + H_2O$	-0.48
$CO_2 + 6H^+ + 6e^- \rightarrow CH_3OH + H_2O$	-0.38
$CO_2 + 8H^+ + 8e^- \rightarrow CH_4 + 2H_2O$	-0.24

From the above scheme it is clear that CO_2 photo reduction is not a single-step reaction. Upon transfer of one electron, the structure changes from linear to bent which results in irreversible reduction (Aulice and Viswanathan ,2004).Additionally, single electron transfer to CO_2 is highly endergonic, because of the negative adiabatic electron affinity of CO_2.

The initial step in the photo catalytic reduction of CO_2 is the generation of electron-hole pairs upon absorption of photons of energy greater than or equal to the band gap of the

photo catalyst. The time scale of this electron-hole recombination is two to three orders of magnitude faster than other electron transfer processes. Therefore, any process which inhibits electron- hole recombination would greatly increase the efficiency and improve the rates of CO_2 photo reduction. The kinetics of CO_2 photo reduction are also dependent upon many other factors such as incident light intensity, fraction of the incident light absorbed by the photo catalyst, the specific surface area of the photo catalyst absorbing the light, etc.

1.7.2 Effect of wavelength, band gap, and light intensity

Semiconductors absorb light radiation with the threshold wavelength that provides sufficient photon energy to overcome the band gap between the valence and conduction bands. This threshold wavelength, required to promote the excited state, corresponds to the minimal photon energy and depends on the band-gap energy, e.g. for TiO_2 anatase with bandgap energy 3.2 eV it is 387.5 nm (Koci *et al*.,2008).

The light wavelength influences the yield of CO_2 photo catalytic reduction products; irradiation using the light with shorter wavelength (254 nm) is significantly more effective for the CO_2 reduction using TiO_2 than that with the wavelength of 350 nm (Matthews and McEvoy, 1992).

Electron excited states are produced via electronic transitions the probability of which depends on the light intensity. At low light intensities, the CO_2 reduction rate increases linearly with the light intensity, at mid-range light intensities, the photo catalytic reaction rate is dependent on the square root of light intensity; and at high light intensities the rate is independent of the light intensity (Koci *et al*.,2008).

Large-band-gap semiconductors are the most suitable photo catalysts for CO_2 reduction, because they provide sufficient negative and positive redox potentials in conductance bands and valence bands, respectively. The disadvantage of using wide band-gap semiconductors is the requirement for high energy input (Somnath *et al*.,2010).

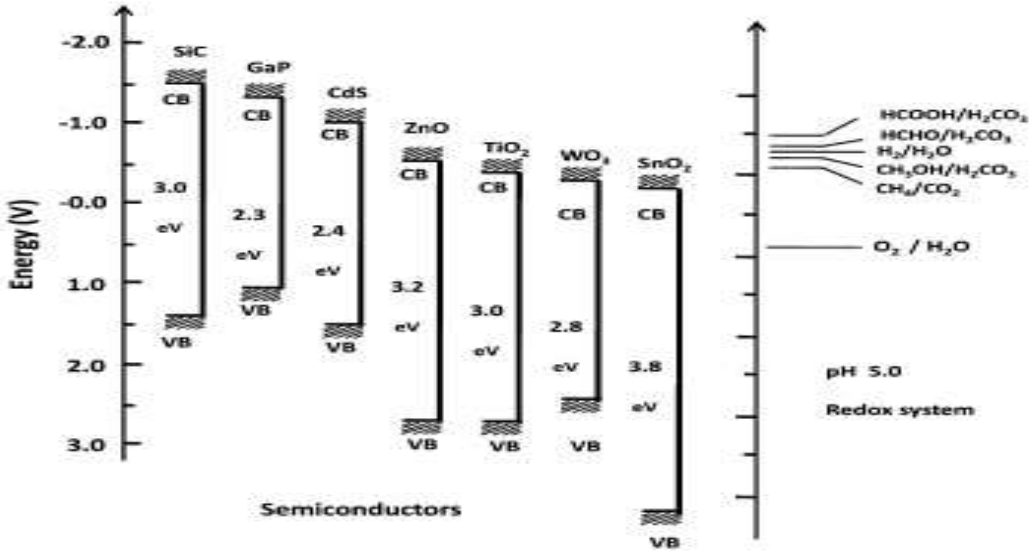

Fig 1.1. Conduction band and valence band potentials of semiconductor photocatalysts relative to energy levels of the redox couples in water .

Although many semiconductors have smaller band gaps and absorb in the visible range (e.g. CdS and Fe_2O_3 with band-gap values of 2.4 and 2.3 eV, respectively), just a few of them are catalytically active because the energy levels of either the conduction or valence bands are unsuitable for CO_2 reduction and/or water oxidation. This limitation, together with poor photo-corrosion stability of many semiconductors, limits significantly the number of potential photo catalytic materials.

CHAPTER 2

PHOTOCATALYTIC REDUCTION OF CO_2 WITH WATER- STATE OF THE ART

Inoue *et al.*(1979) were the first to report the photo catalytic reduction of CO_2 in aqueous solutions to produce a mixture of formaldehyde, formic acid, methanol and methane using various wide-band-gap semiconductors such as tungsten trioxide (WO_3), titanium-dioxide (TiO_2), zinc oxide (ZnO), cadmium sulfide (CdS), gallium phosphide (GaP), and silicon carbide (SiC). These semiconductors were activated by both xenon and mercury-lamp irradiation. The formaldehyde and methyl alcohol yield was highest in the presence of SiC, a behavior attributed to the relative position of the SiC conduction band with respect to the $HCHO/H_2CO_3$ redox potential. The SiC conduction band edge lies at a higher position (more negative) than the $HCHO/ H_2CO_3$ redox potential, which is believed to be responsible for the high rates of product formation. The absence of methyl alcohol when WO_3 was used as catalyst, with a conduction band at a position lower than the $HCHO/H_2CO_3$ redox potential, further indicates the influence of band-edge positions on CO_2 reduction (Fig.1.1).

Investigations related to the photosynthesis reaction of CO_2 with water vapor to form CH_4 over metal-loaded $SrTiO_3$ have also been conducted. Due to its higher conduction band-edge position compared to the redox potential of CH_3OH/H_2CO_3, strontium titanate could effectively reduce carbon dioxide dissolved in an aqueous electrolye (Halmann *et al*.,1983).

Halmann et al .(1984) studied the effect of doping transition and noble metals such as Ru, V, Cr on TiO_2. He found that the production rate of organic compounds such as formic acid, formaldehyde and methanol increased when TiO_2 was doped with RuO_2. The highest initial energy conversion obtained was found to be 0.04%.

Anpo *et al.* (1995) studied the photo catalytic reduction of CO_2 with H_2O on various titanium oxide catalysts. The anatase-type TiO_2 catalyst with large band gap and

numerous surface –OH groups showed high efficiency for the formation of methane. The yields of the photo catalytic reactions depended strongly on the kind of catalyst, the ratio of CO_2 to H_2O and the reaction temperature. He observed that the best mole ratio of H_2O /CO_2 for the conversion of carbon dioxide is 5. Addition of Pt to the TiO_2 led to an increased methane yield compared to methanol formation. In another report Anpo *et al.* (1992) reported the use of highly dispersed titanium oxide on glass for the photo catalytic reduction of carbon dioxide. From the direct detection of intermediate species, they proposed that methane formation resulted from the reaction between carbon radicals and atomic hydrogen.

The use of Cu as a co-catalyst was reported by Adachi *et al* (1994) in which Cu-loaded TiO_2 powder was suspended in a CO_2 pressurized solution at ambient temperature, with methane and ethylene produced under Xe lamp illumination. Tseng *et al* (2004) also studied the effect of copper loading on titania. The methanol yield of 2.0 wt.% Cu/TiO_2 was 118 μmol/g following 6 h of UV illumination. The yield was much higher than those of sol–gel TiO2 and Degussa P25 . The redistribution of the electric charge and the Schottky barrier of Cu and TiO_2 facilitates electron trapping via supported Cu. The photocatalytic efficiency of Cu/TiO_2 was markedly increased because of the lowering the re-combination probability for hole–electron pairs. The highest quantum and energy efficiencies achieved were 10 and 2.5%, respectively. Slamet *et al* (2005) suggested that CuO may be the most active dopant compared to the other copper species. Because Cu_2O has the highest positive potential redox value of Cu^+, Cu_2O dopant should effectively act as an electron trapper to prohibit electron–hole recombination. However, owing to the relatively strong interaction between TiO_2 and the dopant particle implanted in the vacant sites of TiO_2, the dopant with more positive potential redox exceedingly catches electron from conduction band edge. Consequently the dopant-trapped electrons are more difficult to be transformed to the adsorbed species on catalyst surface and hence it may play a role as a center of electron–hole recombination.

Guan *et al.*(2003) studied the reduction of CO_2 with water over a hybrid catalyst, in which a Pt-loaded $K_2Ti_6O_{13}$ photo catalyst was combined with a Fe-based catalyst supported on a dealuminated Y-type zeolite (Fe-Cu-K/DAY). In this reaction system, the

$Pt/K_2Ti_6O_{13}$ catalyst decomposes water to produce H_2 and the Fe-Cu-K/DAY catalyst reduces CO_2 with the resulting H_2 into organic compounds. When the reaction temperature is increased from room temperature to 600K by concentrating the solar irradiation, the product yield of hydrogen increased from 13.7μmol/g-h to 20.5 μmol/g-h. Also additionally formic acid, methanol and ethanol were obtained. Guan *et al* (2003) also reported the use of Pt-loaded $K_2Ti_6O_{13}$ photo catalyst combined with a CO_2 hydrogenation catalyst Cu/ZnO. When the composite catalyst was used under concentrated sunlight, CH_3OH was successfully formed in addition to the above products.

Guan *et al* (2003) also investigated reduction of CO_2 over zero-valent Fe^0 and Fe^0-based composites in an aqueous solution at room temperature. It is found that H_2 can be effectively evolved from water over zero-valent Fe^0 in the presence of gaseous CO_2 together with a small amount of hydrocarbons. When the Fe^0 was combined with Cu, K, and Al components, hydrocarbons such as CH_4 and C_3H_8 and alcohols such as CH_3OH and C_2H_5OH were also effectively produced. The XPS, XRD, and photoemission yield measurements revealed that the Fe^0 surface as well as the bulk was oxidized to Fe_3O_4 and other possible oxides during the reaction. This corrosion process is promoted by the dissolution of CO_2 in water and the resultant protons oxidize Fe^0 to evolve H_2. Moreover, the evolved H_2 serves as the reactant for the CO_2 hydrogenation on the active site of Fe^0, especially for the Fe^0–K–Al and Fe^0–Cu–K–Al composites.

Kaneco *et al* (1997) studied the CO_2 photoreduction using TiO_2 powders in liquid CO_2 medium. Carbon dioxide has an limited solubility in water. Also reduction of CO_2 is competitive with hydrogen formation via water. To overcome this disadvantage liquid CO_2 system has been explored. The protonation reaction was performed using water after the end of illumination. The main reduction product was exclusively formic acid.

Tan *et al* (2006) studied the photo catalytic reduction of carbon dioxide using TiO_2 pellets. Pellet increased the contact areas and adsorption capacity. Their yield was significant when compared to thin film coating technique.

Koci *et al* (2009) studied the effect of TiO_2 particle size on photo catalytic reduction of carbon dioxide. As the particle size decreased, higher yields of methanol and methane over the TiO_2 nano particles under the illumination of light were obtained. The optimum particle size corresponding to the highest yields of both products was 14 nm. For crystal sizes smaller than 14 nm the catalyst activity dropped probably due to the changes in optical and electronic properties of the nanometer crystal. The observed optimum particle size was a result of competing effects of specific surface area, charge–carrier dynamics and light absorption efficiency.

Liu *et al* (2007) reported photo catalytic reduction of carbon dioxide using sol–gel derived titania-supported CoPc catalysts. Cobalt phthalocyanine (CoPc) nanoparticles loaded titania was a highly efficient photo catalyst for CO_2 reduction since photoconductive CoPc is prone to transfer electron to TiO_2 under irradiation, and able to reduce the recombination of electron–hole pairs.

Cho ching *et al* (2007) studied the photo reduction of carbon dioxide with H_2 and H_2O over TiO_2 and ZrO_2 in a circulated photo catalytic reactor. Experimental results indicated that the highest yield for the photo reduction of CO_2 was obtained using TiO_2 with H_2+H_2O and ZrO_2 with H_2. Photo reduction of CO_2 over TiO_2 with H_2+H_2O formed CH_4, CO, and C_2H_6 with the yield of 8.21, 0.28, and 0.20 mmol/g, respectively, while the photo reduction of CO_2 over ZrO_2 with H_2 formed CO at a yield of 1.24 mmol/g. The detected reaction products supported the proposition of two reaction pathways for the photo reduction of CO_2 over TiO_2 and ZrO_2 with H_2 and H_2O, respectively. A one-site Langmuir–Hinshewood (L–H) kinetic model was applied to simulate the photo reduction rate of CO_2.

Koci *et al* (2011) studied the influence of reactor geometry on photoreduction of carbon dioxide using two annular batch reactors. The dependence of products yields on the reactor diameter and on the volume of the liquid phase confirmed the fact that the requirement of perfect mixing is difficult to fulfill in the annular configuration of the reactor. The highest yields of the photo catalytic reduction were achieved in a

configuration where the lamp just touches the surface of the liquid in the reactor and the configuration of the reactor was not annular.

Wu *et al* .(2008) applied an optical fibre reactor to the photo reduction of CO_2 with H_2O using TiO_2,Cu/TiO_2, Ag/TiO_2, $Cu–Fe/TiO_2–SiO_2$ and dye-sensitized Cu–Fe/P25 coated optical fibers. Compared with a traditional packed-bed reactor, an optical fiber provides a medium to transmit light uniformly throughout a reactor. In addition, a higher processing capacity is possible because the photo catalyst can be disperse on the optical fibers with large surface area in a given reactor volume.

Ulagappam *et al* (2000) used Ti-silicalite molecular sieves as a catalyst for 266 nm UV laser radiation induced reduction of CO_2 and H_2O gas mixtures, obtaining HCO_2H, CO, and HCO_2CH_3. Product origins were studied by IR spectroscopy, indicating that CO originated from the secondary photolysis of HCO_2H, while HCO_2CH_3 was the result of spontaneous Tishchenko reaction of CH_2=O.

Anpo *et al* (1997) carried out the CO_2 photo reduction using Ti-MCM-41 and Ti-MCM-48 mesoporous zeolite catalysts. Photo catalysts prepared within the zeolite cavity and framework have a unique local structure and high selectivity in photo reduction. The titanium oxide species included within the zeolite framework have been found to exist as isolated tetrahedral titanium oxide species. These Ti-containing zeolite catalysts exhibited high photo catalytic efficiency and selectivity for the formation of methanol.

Some researchers have attempted to replace water with other reductants. This provides a high reaction yield and high selectivity to desired products by changing the mechanism.
Liu *et al*. (1998) conducted an experiment with CdS in various solvents including water, methanol, ethanol, and 1-propanol with dielectric constants of 80, 33, 24.3, and 20.1, respectively. The results indicated that, if low-dielectric constant solvents or low-polarity solvents are used, $CO_2^{\cdot-}$ anion radicals can be strongly adsorbed on the surface through the carbon atom of another $CO_2^{\cdot-}$ anion radical because these radicals are not well dissolved in low-polarity solvents. Here, CO is produced as the major reduction product of CO_2. If a high-dielectric-constant solvent is used (e.g., water), the $CO_2^{\cdot-}$anion radicals

can be greatly stabilized by the solvent, resulting in weak interactions with the photo catalyst surface. Subsequently, the carbon atom of the radical tends to react with a proton to produce formic acid. Dey (2007) showed that photo-catalytic reduction of CO_2 using TiO_2 suspension in aqueous solutions containing 2-propanol as a hole scavenger leads to the formation of methane.

Titania *per se* is active for photo catalytic reduction of CO_2 with H_2O , but the rates are extremely low since its conduction band edge is not suitable for water and CO_2 reduction, though it can readily oxidize water (Varghese *et al*.,2009). Promotion with co-catalysts like Pt (Zhang *et al*., 2009), Ru (Sasirekha *et al*.,2006), Rh (Kohno *et al*.,1999), Ni (Fan *et al*.,2010) & Ag (Koci *et al* ,2011) vastly enhance the rate in several ways, like, charge separation, retarding re-combination and trapping of charge carriers, besides activation of CO_2 & water reduction and facilitating further surface transformations leading to hydrocarbon products .

Effect of bimetallics on TiO_2 were also studied. Luo *et al.* (2011) studied the CO_2 reduction on Copper and Cerium Co-Doped Titanium dioxide. Photo catalysits copper and cerium co-doped titanium dioxide were prepared via the equivalent-volume incipient wetness impregnation method. The methanol yield could reach up to 180.3 μmol/g-cat rapidly. Ce atoms activated H_2O and CO_2 molecules, while Cu atoms act as the channel of photoelectrons in real time and prevent the recombination of electrons and holes.

Xia *et al* (2007) studied the reduction of CO_2 with H_2O using multi-walled carbon nanotube supported [MWCNT] TiO_2.They were prepared by both sol gel and hydrothermal method. In using the sol–gel method, the MWCNTs were coated with anatase TiO_2 nanoparticles, and by the hydrothermal method, rutile TiO_2 nanorods were uniformly deposited on the MWCNTs. The composite catalysts prepared by the sol–gel method lead to the main formation of C_2H_5OH, while HCOOH is found to be the major product on the sample prepared by the hydrothermal method.

When CO_2 present in the atmosphere dissolves in water it is mostly present in the formation of carbonate. Many of them have studied photo catalytic reduction of carbonate

to form various chemicals. Ku et al (2004) studied the photo catalytic reduction of carbonate in aqueous solution by the UV/TiO_2 process. The photo catalytic reduction of carbonate proceeded faster in acidic solutions than in alkaline solutions. The main products of the photo catalytic reduction of carbonate by the UV/TiO_2 reduction process were found to be methanol and methane. A Langmuir–Hinshelwood type kinetic equation was developed for modeling the photo catalytic reduction of carbonate.

Sayama *et al* (1997) investigated the effect of carbonate salt addition on the photo catalytic decomposition of liquid water over Pt–TiO_2 catalyst. It has been found that an addition of carbonate salts to Pt-loaded suspensions led to highly efficient stoichiometric photo- catalytic decomposition of liquid water into H_2 and O_2 . Neither the pH nor cation directly contributes to the water splitting .The presence of a high concentration of carbonate ions is essential for the catalytic photodecomposition of water. The carbonate ion affects both the Pt particles and the TiO_2 surface. The Pt was covered with some titanium hydroxide compounds and therefore, the rate of the back reaction (H_2O formation from H_2 and O_2) on the Pt was suppressed effectively in the presence of carbonate ions. On the other hand, the TiO_2 surface was readily covered with several types of carbonate species. It is considered that these carbonate species aid desorption of O_2 from the TiO_2 surface.

A significant breakthrough in the photocatalytic reduction of gas phase CO_2 by solar radiation has recently been achieved by Varghese and coworkers (2009), using nitrogen-doped TiO_2 nanotube arrays co-catalyzed with copper and/or Pt nanoparticles, in which water vapor saturated carbon dioxide was reduced to methane and other hydrocarbons under natural sunlight. The yield of methane was reported to be 160 μL/gh.The high rate of carbon dioxide conversion can be attributed to the high surface area and nanoscale wall thickness of the nanotubes, enabling the surface species to readily receive both charge carriers generated near the surface due to the wave function overlap and those generated deep inside the wall *via* diffusion. The quantum efficiency was found to be 0.74 %.

Many researchers have studied the Photocatalytic reduction of CO_2 using external hydrogen. Tsuneok *et al* (2010) performed this over MgO, CaO, ZrO_2, Ga_2O_3, and Al_2O_3. Ga_2O_3 exhibited the highest photo catalytic activity in this process, and CO gas was selectively generated at room temperature and atmospheric pressure. The amount of CO gas evolved depended not only on the amount of CO_2 but also on the amount of H_2 adsorbed on Ga_2O_3. The chemisorbed CO_2 species involved in the photo catalytic reduction of CO_2 over Ga_2O_3 was not the bidentate bicarbonate species but the mono dentate bicarbonate species. The dissociatively adsorbed hydrogen on Ga_2O_3 reduced the mono dentate bicarbonate to the bi dentate formate under photo irradiation. The bi dentate formate, which was an intermediate in the photocatalytic reduction, decomposed to CO. They proposed that photo catalytic reduction of CO_2 over Ga_2O_3 takes place via a Langmuir-Hinshelwood-type mechanism, which is not the case for ZrO_2 or MgO.

Teramura *et al* (2010) carried out the Photocatalytic reduction of CO_2 using H_2 as reductant over $ATaO_3$ photocatalysts [A = Li, Na, K]. Only CO gas was generated over all samples under photo irradiation. The photocatalytic activity was higher in the order corresponding to $LiTaO_3 > NaTaO_3 > KTaO_3$. The order of the photo catalytic activities was consistent with that of the Eg [optical gap] values. The amount of evolved CO gas almost strongly depends on the amount of chemisorbed CO_2 in the case of $ATaO_3$ [A = Li, Na, K]. In addition, the photo catalytic activity increased with increasing the calcination temperature of $LiTaO_3$. This means that a smooth charge separation in a $LiTaO_3$ photo catalyst and chemisorption of CO_2 on the surface contribute to effective reduction of CO_2 in the presence of H_2.

Catalyst systems other than TiO_2 were also intensively studied.
M Watanabe *et al.* (1992) studied the Photosynthesis of methanol and methane from CO_2 and H_2O molecules on a ZnO surface. The photochemical synthesis of methanol and methane from CO_2 and H_2O molecules was observed at 5°C by irradiating ZnO powder with visible light under high pressures of 25 to 35 kg/cm^2 of CO_2, gas. The best conversion efficiency was found to be about 6% with respect to reactant H_2O molecules using a 75 W Xe lamp.

M Kanemoto *et al* (1992) studied the photo reduction of Carbon Dioxide over ZnS Quantum Crystallites. The dissolution of CO_2 in water gives an aqueous solution of pH 3.7 under a pressure of 1 atm. ZnS is unstable under acidic conditions, decomposing into H_2S and Zn^{2+} by the reaction with acid. Freshly prepared colloidal ZnS suspensions effectively catalyze photo reduction of CO_2 in water at pH 7 with NaH_2PO_2 in the coexistence of Na_2S under UV irradiation.

Y.Wang *et al* (2010) carried out the Photocatalytic H_2 evolution from water in the presence of Carbon dioxide over $NiO/Ca_2Fe_2O_5$. The catalyst $NiO/Ca_2Fe_2O_5$ was studied in the photo catalytic splitting of water in the presence of carbon dioxide. It is believed that CO_2 may react with water to form HCO^-_3 and CO_3^{2-}, which promote the scavenging of holes by OH, and thus enhance the photocatalytic activity. At the same time, a portion of CO_2 is photo catalytically reduced to formic acid.

Ahmed *et al* (2011) studied the Photocatalytic conversion of carbon dioxide into methanol using zinc–copper–M[III] [M = aluminum, gallium] layered double hydroxides. These LDH compounds were applied as photo catalysts to convert gaseous CO_2 [2.3 kPa] to methanol or CO under UV–visible light using hydrogen. Zn Al LDH was the most active for CO_2 photo reduction and the major product was CO formed at a rate of 620 nmol $h^{-1}g^{-1}$ cat, whereas methanol was the major product formed by the inclusion of Cu in the LDH photo catalysts, e.g., at a formation rate of 170 nmol $h^{-1}g^{-1}$cat using Zn-Cu-Ga photo catalyst.

Yan *et al* (2010) studied the CO_2 photo reduction using meso porous $ZnGa_2O_4$. a reactive templating route to preparing meso porous $ZnGa_2O_4$ at room temperature has been reported. By using RuO_2 as co-catalyst, the as-prepared meso porous $ZnGa_2O_4$ shows high photo catalytic activity for converting CO_2 into CH_4 under light irradiation, because of strong gas adsorption and large specific surface area of the mesoporous photo catalyst.

2.1 AIM AND SCOPE OF CURRENT INVESTIGATION

As described in the earlier Chapter, photo catalytic reduction of carbon dioxide with water to fuels/chemicals (methane, methanol, etc.,) is an emerging area of research towards utilizing the abundant sunlight. The process has the potential to become a viable and sustainable alternative energy source to fossil fuels. However, it has thrown up several tough challenges to the scientists & technologists, namely,

- The process centers around the activation of two thermodynamically most stable molecules, CO_2 and water
- Conversions achieved so far are extremely small, < 1 %, occurring at very slow rate
- Catalysts tend to get deactivated over short period
- CO_2 photo reduction process is highly complex, involving multi electron transfer and non-selective, leading to a range (C_1-C_3) of hydrocarbon products
- Design of catalysts, consisting of photo catalysts and co-catalysts aided by metal ion / anion doping and light harvesting components/sensitizers, is equally complex.
- Ideal catalysts are expected to display maximum efficiency towards solar energy absorption and possess requisite band energy level characteristics to drive the redox reactions.
- The process involves two steps, spitting of water and reduction of carbon dioxide, which is thermodynamically more favourable. Since the second step involves multi-electron transfer, the rates are very slow relative to the first. These two steps are to be synchronized to achieve higher yields of hydrocarbons.

Nevertheless, research efforts on these fronts are being pursued with full vigour by many laboratories round the globe. Design of efficient catalyst systems and achieving higher yield of desired products are the two key issues being pursued by the researchers.

The objective of the current investigation is to explore new catalyst formulations that can improve hydrocarbon yields from CO_2 and water. The catalyst systems investigated so far include:

- Titania and its various modified versions- metal loaded (Pt,Ag,Cu,Ru), anion doped (N,S,C), coupled with other semi-conductors (NiO,CuO), different crystallographic modifications, as films, nano tubes and in other specific nano structures
- Titania dispersed in high surface area ordered meso porous matrices, MCM-41, Ti Silicalite, Zeolite beta , in mixed oxides with Si, Zr
- Metal oxides/ sulfides /metal-oxide hetero structured composites (of Fe,Bi Zn & CdS)
- Ru & Co bypyridine complexes, metallo phthalocyanins,coupled with dye sensitizers
- Alkaline earth titanates (Sr TiO_3) & layerd titanates ($K_2Ti_6O_{13}$)

A general characteristics that all these catalysts possess is the ability to generate hydrogen by photocatalytic splitting of water, which is the primary step in CO_2 photoreduction as well. The second and the most crucial step is the reduction of CO_2 to hydrocarbons. As illustrated in the previous Chapter, for this step, the energy level of the conduction band has to be more negative with respect to reduction potential for CO_2.

It is observed that alkali and alkaline earth tantalates and niobates,which satisfy both these criteria have not been explored for CO2 photoreduction with water. Hence $NaTaO_3$ and $KTaO_3$ have been selected for studies in this work.

Similarly, layered titanates, $Sr_3Ti_2O_7$ & $La_2Ti_2O_7$, which are active for water splitting and possess conduction band energy levels suitable for CO_2 reductive conversion have been taken up for investigations . These systems have not been explored for CO_2 photo reduction.

In an effort to explore further improvements in titania based catalysts, studies have been undertaken on

- Comparison of the performance of standard P-25 titania with another cmmercial titania and titania samples prepared by sol-gel methods
- Effect of metal loading, as revealed by loading of Pt & Ag
- Effect of using CuO & NiO as coupled semi-conductors with TiO_2

Accordingly the work plan is focussed on preparation, photo-physical characterization and evaluation of activity for phot reduction of CO_2 by water on the following catalyst systems:

- Comparison of the performance two commercial titania samples, P-25 & Hombikat- UV-100
- Studies on TiO_2 samples prepared by sol-gel methods, adopting two different alkoxide hydrolysis routes- acetic acid esterification and reverse micelle.
- Effect of metal loading (Pt & Ag) and coupled semiconductors (CuO & NiO) on titania.
- Preparation of $NaTaO_3$ and NiO/La:$NaTaO_3$ and comparison of activities for CO_2 photo reduction.
- Preparation of $Sr_3Ti_2O_7$ and NiO/Ba:$La_2Ti_2O_7$ and to study the ability of these systems to reduce CO_2

It is hoped that an understanding of the photo catalytic activity of these systems in terms of their solid state & photo-physical characteristics and the underlying reaction mechanism would lead towards development superior catalysts.

CHAPTER 3
EXPERIMENTAL METHODOLOGY

3.1 CHEMICALS AND MATERIALS

Titanium (IV) isopropoxide was obtained from Spectrochem ,India . Triton X -114 , hexa chloro platinic acid ,nickel nitrate and copper nitrate were obtained from Sigma Aldrich. Tantalum (V) oxide was purchased from Alfa Aesar. Barium nitrate and silver nitrate were procured from SD fine chemicals. Lanthanum oxide was procured from Loba chemie. P25 (commercial TiO_2) was obtained from Degussa, Germany . Hombikat UV 100 (commercial TiO_2) was purchased from Sachtleben ,Germany. All other chemicals used in the investigations were of analytical (AR) grade and were obtained from Sisco Research Laboratories Pvt. Ltd. or S.D. Fine Chemicals, India.

3.2 PREPARATION OF CATALYSTS

3.2.1 Preparation of TiO_2 and Ag (7 %) loaded TiO_2 by inverse micelle method

Pure TiO_2 and silver loaded TiO_2 powder were prepared by the sol–gel process controlled in the inverse micellar environment (Koci *et al*,2011). Pure TiO_2 was synthesized by the addition of titanium (IV) isopropoxide into formed inverse micellar solution made of cyclohexane, nonionic surfactant Triton X-114 and distilled water. The molar ratio of cyclohexane : Triton : water : Titanium isopropoxide was kept at 11:1:1:1. Inverse micelles of water in, Triton X-114 dispersed in cyclohexane was prepared in a beaker by taking appropriate amounts of cyclohexane, Triton X-114 and water. The suspension was stirred intensively for 15 min for homogenization and formation of micelles Then liquid Titanium (IV) isopropoxide was added drop by drop into the micellar solution during the vigorous stirring. During the addition of isopropoxide the sol changed the state from transparent to viscous yellow. After the addition of all the isopropoxide the sol was stirred for another 10 min. Lastly, the sol was left in a bowl exposed to air for 24 h. The obtained rigid gel was calcined at 400°C for 4 hrs. in a muffle furnace.

Ag loaded titania was similarly prepared, by adding silver nitrate solution (1.85 M) instead of distilled water to get Ag (7%) loaded TiO_2.

3.2.2 Preparation of TiO_2 by sol gel method

Titanium isopropoxide (25 ml) was added to acetic acid (48 ml) with stirring. Water (150 ml) was added to the mixture drop-wise with vigorous stirring. (The titanium isopropoxide, acetic acid and water are in 1:10:100 molar ratios.) The solution was stirred for 8 h to get a clear transparent sol and allowed to dry at 100°C, after which it was calcined at 600°C in air for 2 h at a ramp rate of 5°C/min to get TiO_2 (sol gel) (Seery *et al*.,2007)

3.2.3 Preparation of Pt (0.1 %) loaded TiO_2 (P25) catalyst

Pt loaded TiO_2 (P25) catalyst were prepared by incipient wet impregnation method (Zhang *et al*., 2009) with an aqueous solution of hexa chloro platinic acid ($H_2PtCl_6.6H_2O$) . 0.5 ml of hexa chloro platinic acid solution was taken based on Pt content in the sample (0.1 wt.%). It was then mixed with 9.99g of P25 in round bottom flask. The resulting slurry was stirred with controlled heating at 60°C for 2 h and maintained at 90°C for 30 min to evaporate the water completely. The solid residue is further dried at 110°C for 12 h and calcined in air at 500°C for 2 h. Before the CO_2 photo reduction reaction, it was reduced in H_2 at 450°C for 3 h (Zhang *et al*., 2009).

3.2.4 Preparation of CuO(3 %) loaded TiO_2 (P25) catalyst

CuO(3 %) loaded TiO_2 (P25) catalyst was prepared by impregnating copper nitrate solution on P25 catalyst . Appropriate amount of P25 and copper nitrate solution was taken together and sonicated for 1 h and then stirred for 4 hrs at 95°C. It was then dried at 150°C for 2hrs at a ramp rate of 3°C/min .The dried sample was then calcined at 500°C for 0.5 h at the ramp rate of 5°C/min to obtain CuO(3 %) loaded TiO_2 (Slamet *et al* ,2005).

3.2.5 Preparation of NiO (6 %) loaded TiO_2 catalyst

NiO loaded TiO_2 catalyst were prepared by sol gel method. First Titanium isopropoxide and isopropanol were mixed and stirred for 30 min at room temperature. Acetic acid and appropriate amount of nickel nitrate was then added into the solution. The resulting mixture was stirred for 8 hrs. The solution was aged until sol was formed. The sol was put in vacuum for 10 hrs at a temperature of 75°C. The resulting sample was calcined at 500°C for 30 min to get NiO (6 %) loaded TiO_2. (Fan *et al*.,2010)

3.2.6 Preparation of $NaTaO_3$ and La (2 %) substituted $NaTaO_3$

Synthesis of $NaTaO_3$ was attempted through both (a) hydrothermal route (Li *et al*.,2009) and (b) solid state route (Kato *et al*.,2003). (a) 0.60 g of NaOH dissolved in 20 ml of water (0.75 M) and 0.442 g of Ta_2O_5 were added into a Teflon-lined stainless steel autoclave .The autoclave was heated at 140°C for 12 hrs. The resulting precipitate was collected and washed with deionized water and ethanol several times to remove excess sodium. It was dried at 80°C for 5 hrs. (b) Starting materials Na_2CO_3, Ta_2O_5 were mixed according to the ratio Na:La:Ta= 1.05:1.The mixture was calcined in air at 1147°C for 10 h. The excess amount of sodium was washed with water. Then the powder was dried at 47°C for 2-12 hrs in air to get $NaTaO_3$.

La (2 %) substituted $NaTaO_3$ was prepared by hydrothermal method analogically, however 0.0065 g of La_2O_3 was added along with the other compounds in the autoclave. NiO (0.1 %) co catalyst was loaded to La substituted $NaTaO_3$ by an impregnation method from an aqueous solution of $Ni(NO_3)_2.6H_2O$. Water was evaporated on a oil bath. The dried powder was calcined at 267 °C for 1 h in air to obtain NiO(0.1%)/La: $NaTaO_3$.

3.2.7 Preparation of NiO(2%)/Ba (8%):$La_2Ti_2O_7$

Ba subsituted $La_2Ti_2O_7$ was prepared by solid state method (Kim *et al*.,2005).Starting materials La_2O_3,TiO_2 (anatase),$Ba(NO_3)_2$ were ground in ethanol and dried in oven. The dried powders were calcined at 1000°C for 10 hrs to obtain Ba (8%):$La_2Ti_2O_7$.Calcined

sample was loaded with NiO (2%) by incipient wetness impregnation method. NiO (2 %) cocatalyst was loaded to Ba-$La_2Ti_2O_7$ by an impregnation method from an aqueous solution of $Ni(NO_3)_2.6H_2O$.The sample was dried in an oven at 100 °C and calcined at 300°C in air for 1h. The nickel-loaded catalysts were then reduced by H_2 at 500°C for 2 h and then oxidized by air at 200°C for 1 h.

3.2.8 Preparation of $Sr_3Ti_2O_7$

$Sr_3Ti_2O_7$ was prepared by polymerized complex method (Jeong *et al*.,2006).
Titanium isopropoxide was added to a mixture of ethylene glycol and methanol, then citric acid and Strontium nitrate were added to the mixed solution, resulting in a single phase transparent solution. Methanol, Ethylene glycol , citric acid should be in the molar ratio of 1:0.4:0.1. After polyesterification of the single phase transparent solution at 130°C for 20 h, the resulting polymerized complex gel was pyrolyzed at 350°C. $Sr_3Ti_2O_7$ was finally synthesized by heating the precursor at 900°C for 2 h and powder was washed with distilled water to eliminate the residue.
Preparation of $Sr_3Ti_2O_7$ was also attempted through solid state method. $SrCO_3$ and TiO_2 powders with a molar ratio of 3:2 were mixed and the mixture was then calcined at 1100°C for 30 h .

3.3 CHARACTERISATION TECHNIQUES

3.3.1 X-ray diffraction studies

The crystal phase of the catalyst was analyzed by Rigaku X-ray diffractometer using Cu Kα radiation (λ=1.54056 Å) with the scan range of 2θ = 5-90° at a speed of 3°/min.. The crystallite size of the catalyst samples were calculated by the Scherrer's formula (Patterson,1939).

$$t = \frac{K * \lambda}{\beta * \cos\theta} \qquad (3.1)$$

Where t = crystallite size

K = constant dependent on crystallite shape (0.9)

λ = x-ray wavelength (1.54056 Å)

β = FWHM (full width at half maximum)

θ = Bragg's angle

The phase composition of TiO_2 was analyzed using the relative peak intensity of anatase and rutile (Spurr and Myers,1957).

$$F_A = \frac{1}{1+1.26(I_R/I_A)} \quad (3.2)$$

3.3.2 Diffuse reflectance UV-Visible spectrophotometric studies (DRS)

Diffuse reflectance UV-Visible absorption spectra of the catalysts were recorded using a Thermo Scientific Evolution 600 spectrophotometer equipped with a Praying mantis diffuse reflectance accessory.

3.3.3 Surface area measurements

Surface area and pore volume of the catalysts were measured using Micromeritics ASAP2020. Degassing of the sample was done at 373 K for 2 h and at 423 K for 3 h. For adsorption experiments, pure nitrogen was used at liquid nitrogen temperature.

3.3.4 Transmission electron microscopic studies (TEM)

Transmission electron micrographs were recorded using JEOL 3010 model. Few milligrams of the samples (1-2 mg) were dispersed in few mL (1-2 mL) of ethanol by ultrasonication for 15 minutes and a drop of the dispersion was placed on a carbon coated copper grid and allowed to dry in air at room temperature.

3.3.5 Scanning electron microscopic (SEM) analysis

Scanning electron micrographs were recorded using FEI, Quanta 200. The samples in the powder form were taken on the carbon tape and mounted on the SEM sample holder.

3.3.6 Fluorescence analysis

The fluorescence spectra of catalysts were measured by a JY Fluorolog-3-11 spectrophotometer at an excitation wavelength of 260 nm.

3.3.7 Temperature Programmed Reduction studies

Temperature programmed reduction (Micromeritics) experiments of the prepared catalyst were carried out using hydrogen. The hydrogen consumption was recorded with TCD cell while the sample was linearly heated from 50 to 800°C at 10°C/min.

3.4 CO_2 photoreduction reaction conditions

- Reactor volume – 620 ml
- Reaction medium - 400 ml of 0.2 N NaOH .
- Catalyst loaded - 0.4 g .
- CO_2 was bubbled for 30 min.
- Reaction medium was irradiated through a 5 cm diameter quartz window.
- Hg lamp with 77 W power was used.
- The products were analyzed using Clarus 500 Perkin Elmer Gas chromatography - using Poroplot Q, 30 m and the detector is FID.

  Injector Temperature : 250°C

  Column Temperature : 150°C isothermal, Hold – 20 min

  Detector Temperature : 250°C

  Carrier Gas : Nitrogen, 1.5 ml/min.
- Methane (10 % in N_2), methanol, acetone, acetaldehyde, ethanol were injected and their retention time were noted. All the compounds were detected in gas phase. Therefore , all the liquid compound were taken, purged with N_2 and then the gas phase which now contains both the compound and N_2 was injected into the GC for calibration. The amount injected was 0.2 ml.
- During the reaction, gas samples (0.2 ml) were withdrawn every two hours from the reactor and injected into the GC.

The schematic representation of the photocatalytic reactor set up is shown in the fig 2.1.A Glass reactor is used with a Quartz window through which CO_2 medium was irradiated. The reactor was tightly closed with the help of stopcocks during the reaction. The solution in the reactor was continuously stirred by a magnetic stirrer.

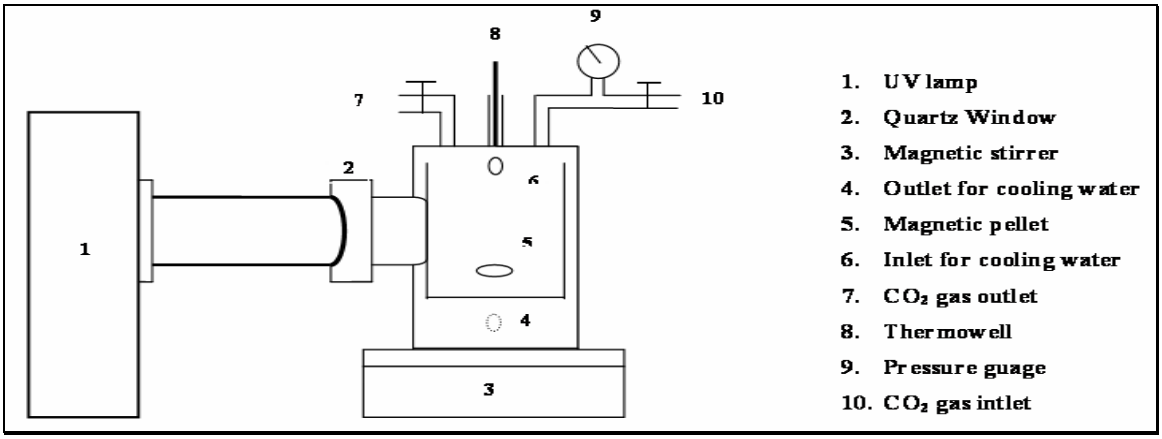

Fig 3.1. Set up of Photocatalytic reactor

Blank experiments were conducted to ensure that the product formed was due to the photoreduction of CO_2. The blank tests consist of a UV-illuminated without the catalyst and a reaction in the dark with the catalyst.

The intensity of the lamp was measured by lux meter and it was found to be 77000 lux which was then converted into Watts with the help of the spectral distribution of the lamp.Using fibre optics spectra analyzer (Ocean optics), the spectral distribution of Hg lamp was found.

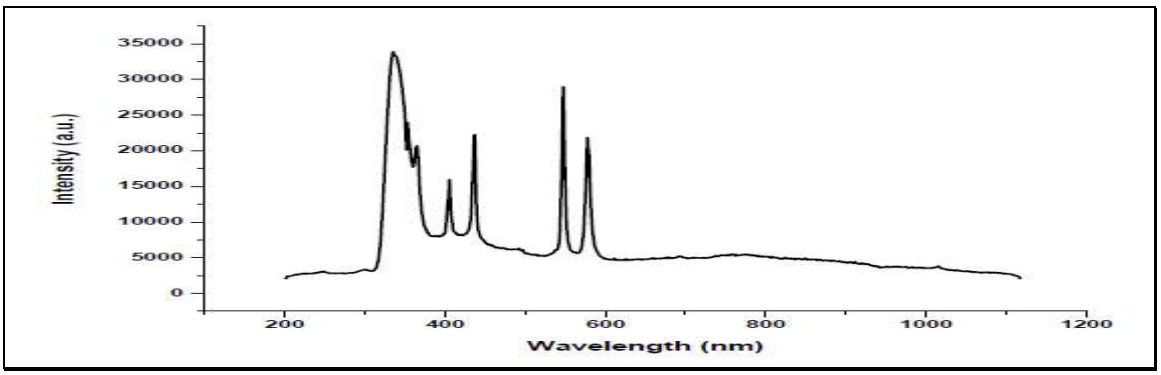

Fig 3.2. Spectral distribution of Mercury lamp

The illumination constitutes 37.3 % of ultra violet radiation (23.8% for λ=335 nm and 14.5% for λ=365 nm) and the remaining visible region.

CHAPTER 4

INVESTIGATIONS ON TiO_2 CATALYSTS

4.1 INTRODUCTION

Titania is considered to be the most practical of the semiconductors for widespread environmental applications such as water purification, wastewater treatment, hazardous waste control, air purification, and water disinfection. Due to its commercial availability, suitable optical and electronic qualities, chemical stability, and nontoxicity, TiO_2 is again found to be the most suitable candidate for photocatalytic conversion of CO_2 as well.

Among the three principal crystalline forms of TiO_2 (i.e. anatase, rutile, and brookite), only the first two are detected in samples synthesized in the usual "soft chemistry" procedures, like sol-gel. Both anatase and rutile are semiconductors with the band gap located at about 3.2 eV and 3.0 eV, respectively. Rutile does absorb some visible light, while anatase only absorbs in the UV region of spectra.

Surface area also plays in an important role in determining TiO_2 activity. In order to enhance the light absorption by titanium dioxide semiconductor, the largest possible surface area of this material is required. Zhang *et al*. (1988) showed that particle size plays an important role in nanocrystalline TiO_2 based catalysts mostly by influencing the dynamics of e^-/h^+ recombination. The band gap of the semiconductor becomes larger with decreasing particle size, i.e., valence band energy (E_{vb}) is moderately shifted to lower energies and E_{cb} is strongly shifted to higher energies (Brus,1986). This is one of the reasons why it is generally possible to control photocatalytic performance by varying the size of the semiconductor particles. Role of surface hydroxyls in activation of water(Hashimoto,2005) ability to adsorb & activate CO_2 (Indrakanti,2009) are the other factors responsible for photo catalysis by titania.

In the present investigation four different samples of titania have been studied for photo reduction of CO_2. Two of them are commercial samples, P25 & HOMBIKAT-UV-100. Other two samples have been prepared in the laboratory, as per the methods described in Chapter 3.

4.2 RESULTS AND DISCUSSION

4.2.1 X-ray diffraction

X-ray diffraction patterns of all the prepared and commercial samples are given in Fig. 4.1. The XRD peaks in Figure 4.1 at 2θ (degree) = 25.28, 37.98, 48.38, 53.98, 55.08, 62.78, 68.98, 70.18 and 75.58 were identified as anatase phase of TiO_2, and the other diffraction peaks at 2θ (degree)= 27.58, 36.18, 41.38 and 48.18 represented rutile phase of TiO_2 structure, using Joint committee on Powder Diffraction Standards (JCPDS) data (Card Nos- 89-4920 and 89-4921)

Except P25, rest of the samples contain pure anatase phase. P25 consists of 85% anatase and the rest rutile.

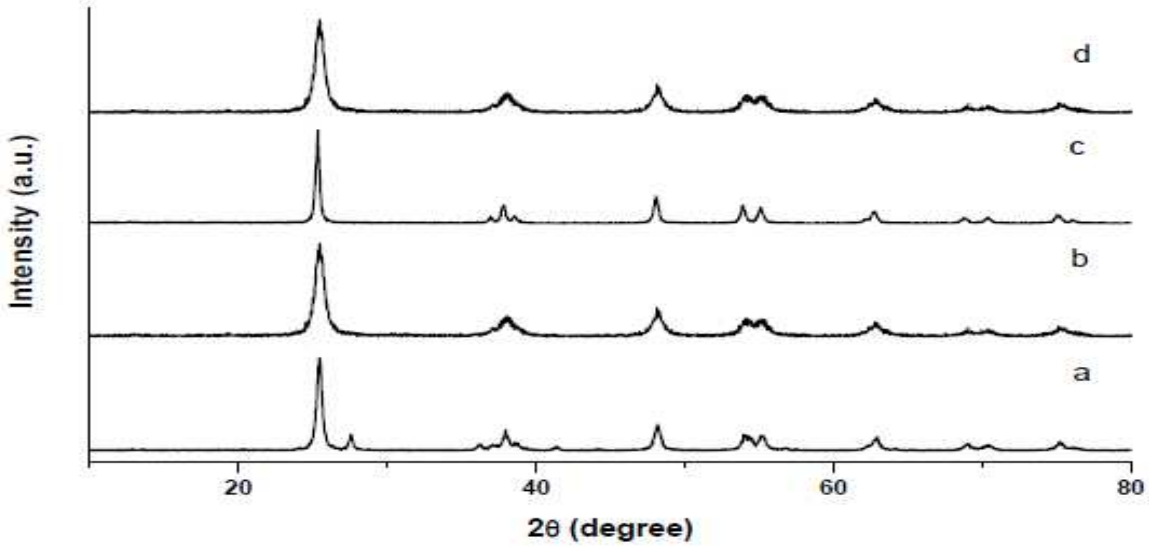

Fig 4.1.X-ray diffraction pattern of (a) P25 (b) TiO_2 (inverse micelle) (c) TiO_2 (sol gel) (d) Hombikat UV100.

The crystallite size of these samples are tabulated below.

Table 4.1. Crystallite size of the titania samples

Catalyst	**Crystallite size (nm)**
P25	22
Hombikat UV100	9
TiO_2 (inverse micelle)	12.3
TiO_2 (sol gel)	27.7

4.2.2 UV -Visible diffused reflectance spectra

Fig 4.2. shows the UV-visible absorption spectra of all the TiO_2 catalysts .The band gap was estimated by extrapolating the rising segment of the UV spectrum to the abscissa at zero absorption .

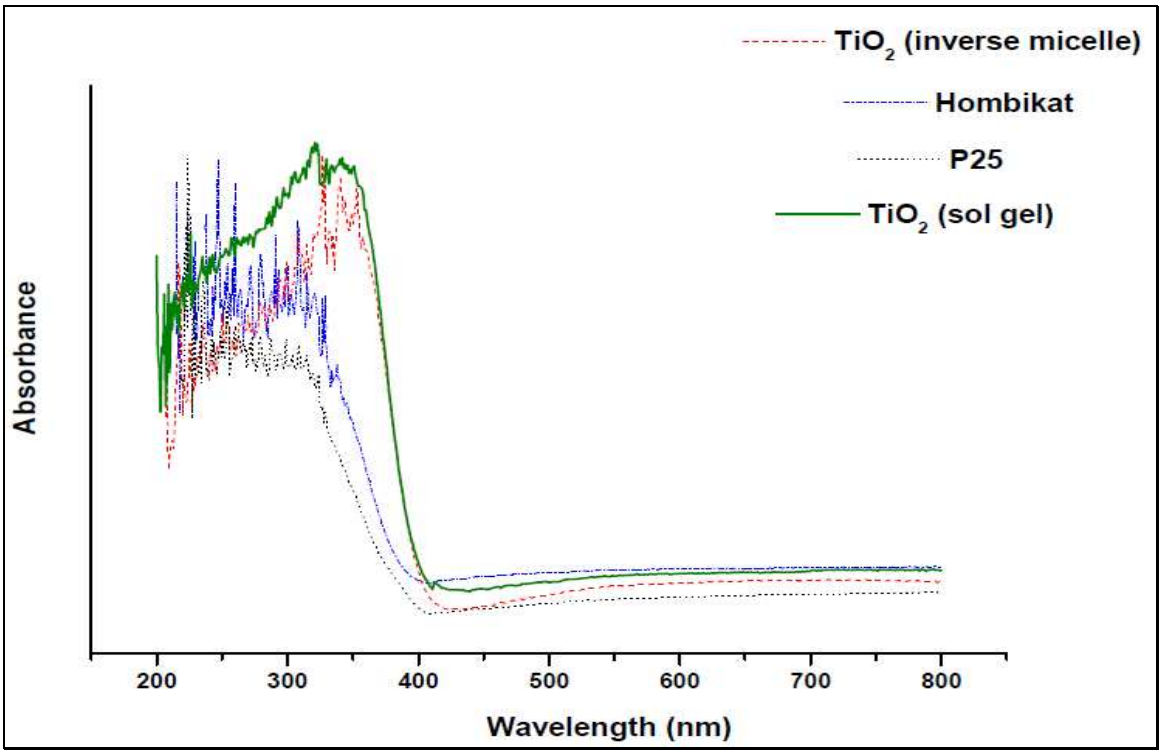

Fig 4.2. UV Vis spectra of P25, TiO_2 (inverse micelle) , TiO_2 (sol gel) , Hombikat .

The band gap values are tabulated below.

Table 4.2. Band gap of the prepared and commercial titanias

Catalyst	**Band gap (eV)**
P25	3.02
Hombikat UV100	3.04
TiO_2 (inverse micelle)	3.06
TiO_2 (sol gel)	3

4.2.3 Surface area measurement

The BET surface area of the titania samples are tabulated below

Table 4.3. BET surface area of materials studied including commercial samples

Catalyst	**BET surface area (m^2/g)**
P25	50.2
Hombikat UV100	311
TiO_2 (inverse micelle)	48.3
TiO_2 (sol gel)	8

4.2.4 Fluorescence analysis

Emissions around 300 nm were observed for excitation at 260 nm. Fig 4.3. presents the fluorescence spectra of P25 and TiO_2 prepared by sol gel method. The fluorescence intensity of P25 is less than TiO_2 sol gel. The fluorescence of titania is caused by the recombination of electron and holes. The decline in fluorescence intensity for P-25 is due to the reduced number of recombination sites on the TiO_2 surface. Fewer recombination sites on the surface lead to slower recombination of electrons and holes, thus a higher photocatalytic activity (Tseng *et al*,2004) .The reduction in recombination in P-25 is due to the co-existing rutile phase, whose valence band & conduction band levels are slightly higher than those for anatase. At the phase interface, such energy levels promote charge separation, thereby reducing fluorescence intensity as shown in Fig.4.7

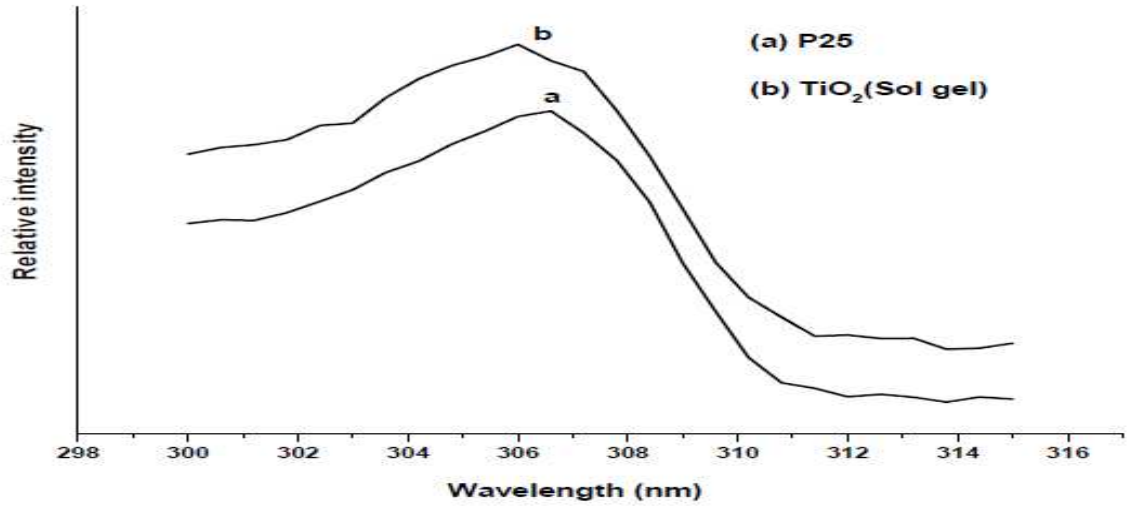

Fig 4.3. Fluorescence spectra of catalysts

4.2.5 Photocatalytic Activity

Photocatalytic reduction of CO_2 has been carried out on these materials under ambient conditions and using 77 W Hg lamp as light source. Fig 4.4 shows the methanol yield of all the catalysts. Fig 4.5 and 4.6 presents the methane and ethanol yield over time for P25 and TiO_2 inverse micelle respectively.

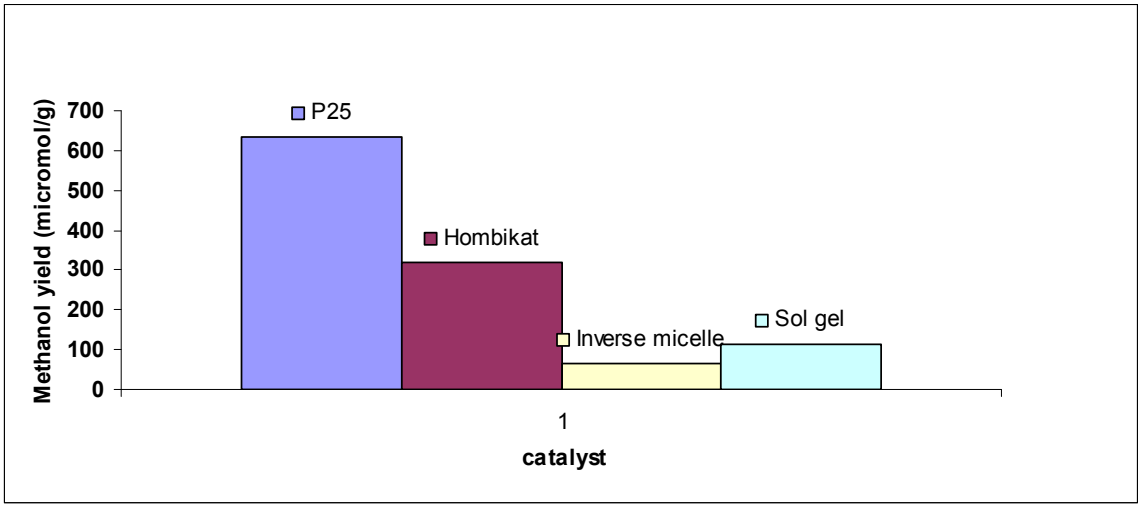

Fig 4.4. Effect of various modifications of TiO_2 on methanol yield.

Only methanol was detected in Hombikat and TiO_2 (sol gel). Among all the titania investigated , TiO_2 (solgel) is found to be the least active catalyst. This is due to its high crystallite size and low surface area. These results clearly illustrate the fact that the mode of preparation of an catalyst plays important role, since it affects the chemical properties of the catalyst .

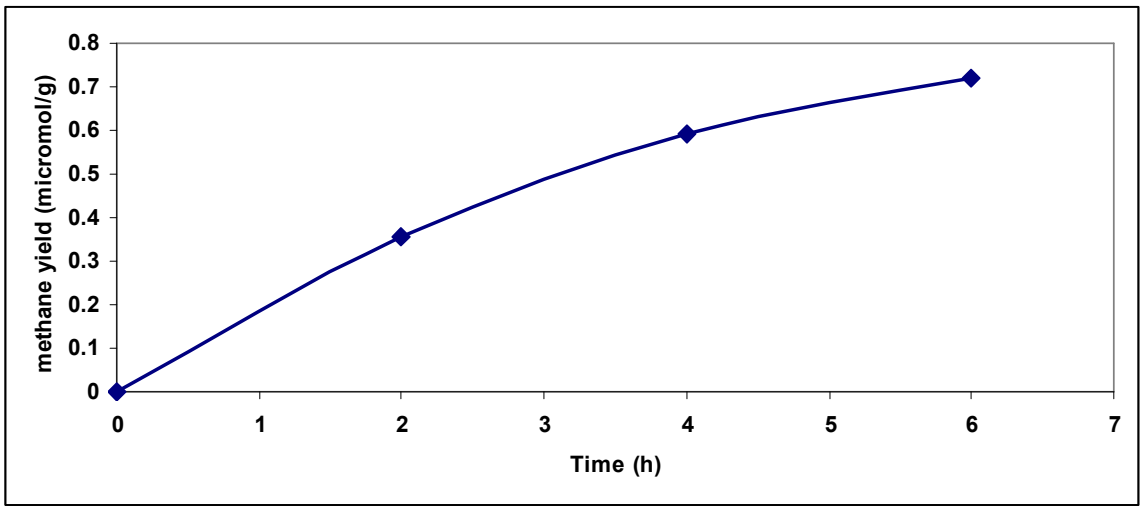

Fig 4.5. Time dependence of methane yield over P25

The measured methane yield at 6th hr is in line with the reported one .(Zhang et al.,2009)

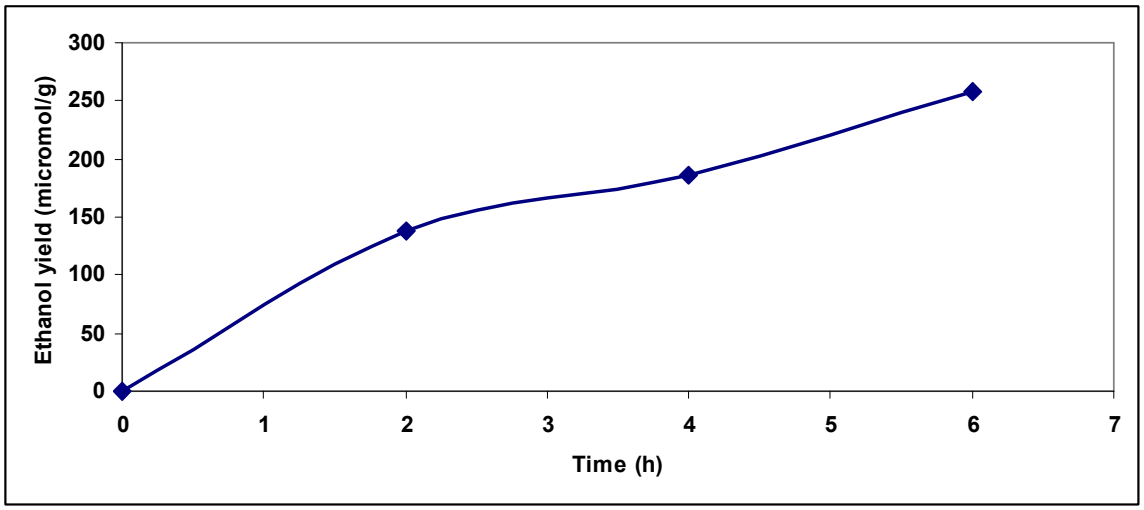

Fig 4.6. Time dependence of ethanol yield over TiO_2 inverse micelle

All the above results clearly indicate that P25 is superior to the other catalysts.

4.2.6 Comparison between P25 and other titania samples.

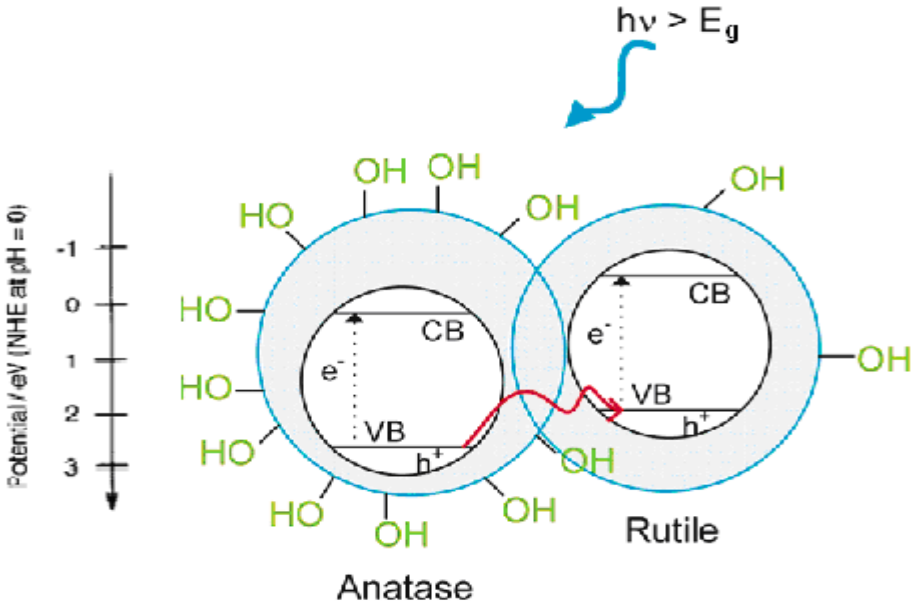

Scheme 4.1. Schemati representation of energy band diagram of anatase and rutile (Carneiro *et al*.,2011)

Titania containing small fractions of the rutile phase show enhanced photocatalytic activity compared to pure anatase, due to electron and hole transfer between the two phases, inducing enhanced lifetimes of electrons and holes. On charge carrier generation by UV excitation in anatase the hole can migrate toward the rutile phase, resulting in longer lifetimes of the conduction band electrons residing in the anatase phase.

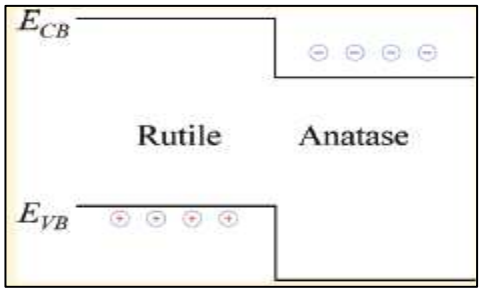

Fig.4.7 Energy levels in mixed phase titania (Deak *et al*.,2011)

Such a charge separation is represented in Fig. 4.7, wherein in a mixed phase titania, electrons are accumulated in conduction band of anatase while holes in valence band of rutile. (Deak *et al*.,2011).

Other reason for the higher activity of anatase is due to higher concentration of surface hydroxyl groups (0.36 mmol/g) relative to rutile (0.07 mmole/g). Surface hydroxyl groups are responsible for the adsorption of water in associative and dissociative forms and facilitate water splitting.

However, HOMBIKAT titania, in spite of having higher surface hydroxyl concentration (1.1mmol/g) is less active possibly due to faster charge recombination.

CHAPTER 5

INVESTIGATIONS ON METAL LOADED TITANIA AND TITANIA COUPLED WITH SEMICONDUCTORS

5.1 INTRODUCTION

To reduce the band-gap energy, doping of TiO_2 with appropriate metal molecules is observed to be a promising method. Doping material can either add an energy level filled with electrons in the band-gap which can be easily excited into the conduction band (n-type) or a level of extra holes in the band-gap to allow the excitation of the valence band electrons, to create mobile holes in the valence band (p-type). Hence, titanium dioxide doping causes sufficient reduction of the TiO_2 band-gap energy allowing the e^-/h^+ pair generation by irradiation with visible light supplying enough energy to generate e^-/h^+ pairs.

In a study of photo induced CO_2 dissociation on titania-supported noble metals (Rasko and Solymosi,1994), it was found that the activity towards CO dissociation correlated with the work function of the polycrystalline metal for titania-supported Pt, Rh and Ir/TiO_2. The following mechanism was proposed to account for photoinduced CO_2 activation on titania-supported noble metal catalysts: Chemisorption of CO_2 on polycrystalline metal islands results in a bent $CO_2^{\delta-}$ species formed by back donation between the metal d-orbitals and the (C–O) Π* orbitals. This electron transfer results in the ‘‘depopulation’’ of the metal surface state. Photogenerated electrons generated upon band gap illumination would be transferred from the conduction band of TiO_2 to the metal island (because the work function of these metals is higher than that of reduced TiO_2).

While metallic promoters are found to be most useful for helping TiO_2 in reduction of CO_2, there exists the possibility of using oxide photcatalysts with appropriate band positions as well, to act as coupled semi-conductors.

In the present investigation, effect of metal loading (Pt & Ag) and presence of coupled semi-conductors in conjunction with TiO_2 have been studied. The wt % of the metal was chosen based on what was reported in the literature as optimal.

5.2 STUDIES ON METAL LOADED TITANIA

5.2.1 Results and discussion

5.2.1.1 X-ray diffraction

X-ray diffraction pattern for the prepared Pt/P25 is given in Fig. 5.1 along with pure P25 for comparison purpose . The crystallite size of the TiO_2 and Pt/TiO_2 samples were calculated by the Scherrer's formula was found out to be 22 nm.

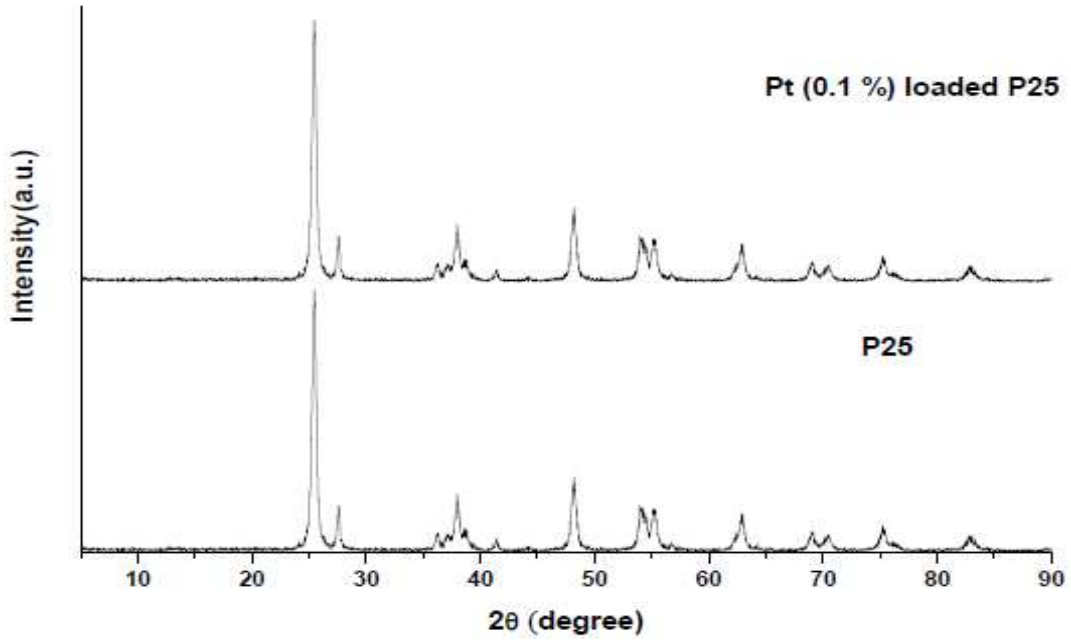

Fig 5.1. XRD pattern of TiO_2 (P25) and Pt/TiO_2.

Based on XRD analysis it was found that addition of platinum to titania did not cause any change in phase composition and crystallite size. This may be due to the very low weight percentage (0.1 %) of platinum loaded on titania.

X-ray diffraction pattern of the Ag/TiO_2 along with TiO_2 (inverse micelle) is given in Fig. 5.2. XRD analysis confirmed the presence of the pure anatase crystallite structure. Ag

was not detected in XRD pattern, probably Ag is situated in the bulk (inside the TiO_2 crystals).The crystallite size was found to be 12.46 nm.

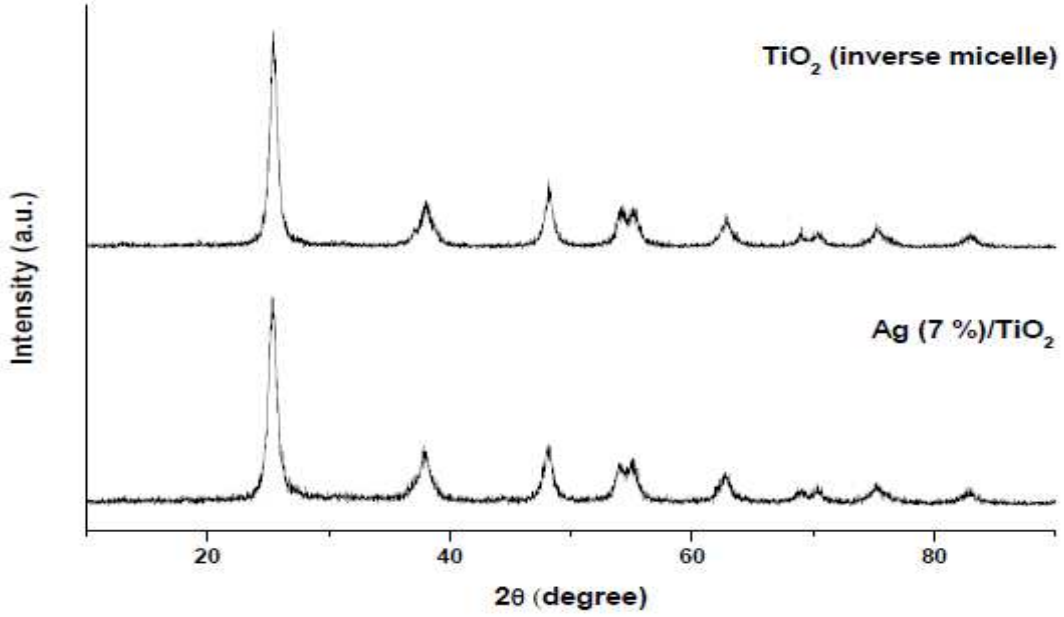

Fig 5.2. XRD pattern of TiO_2 (inverse micelle) and Ag (7%)/TiO_2.

5.2.1.2 UV -Visible spectra

Fig 5.3. shows the UV-visible absorption spectra of TiO_2 and Pt/TiO_2 .

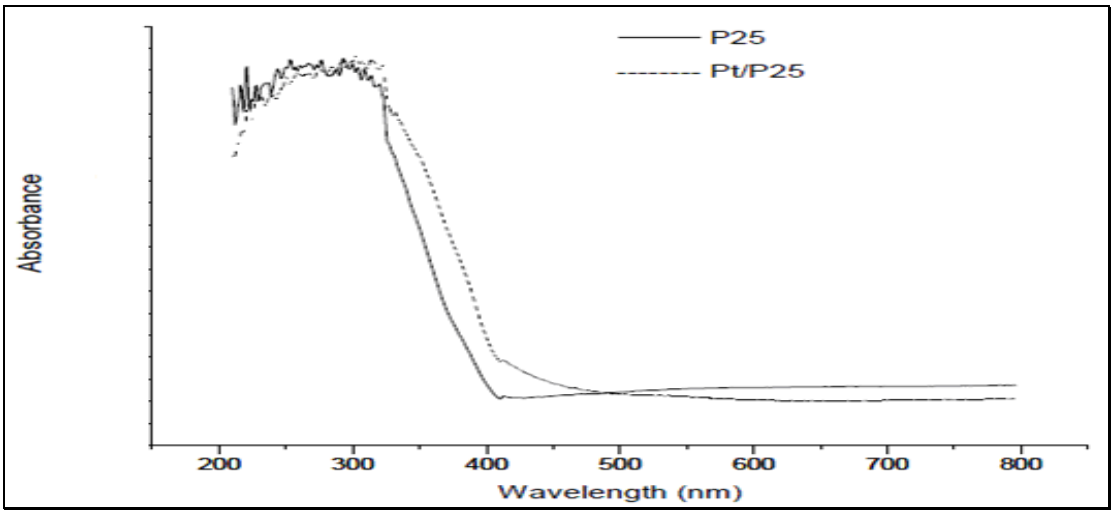

Fig 5.3: UV spectra of TiO_2 and Pt/TiO_2

We can see that TiO_2 absorbs light of wavelength below 400 nm. The UV-visible absorption spectra of Pt/TiO_2 is similar to that of TiO_2. On loading Pt on P25 additional surface state at 3 eV is created.

Fig 5.4. shows the UV-visible absorption spectra of TiO_2 (inverse micelle) and Ag/TiO_2 On loading Ag on TiO_2 additional surface state at 2.61 eV is created which is close to the value reported in the literature. Whereas for pure anatase TiO_2 , the band gap was 3.06 eV. The absorption was shifted into the visible region for Ag/TiO_2 catalysts.

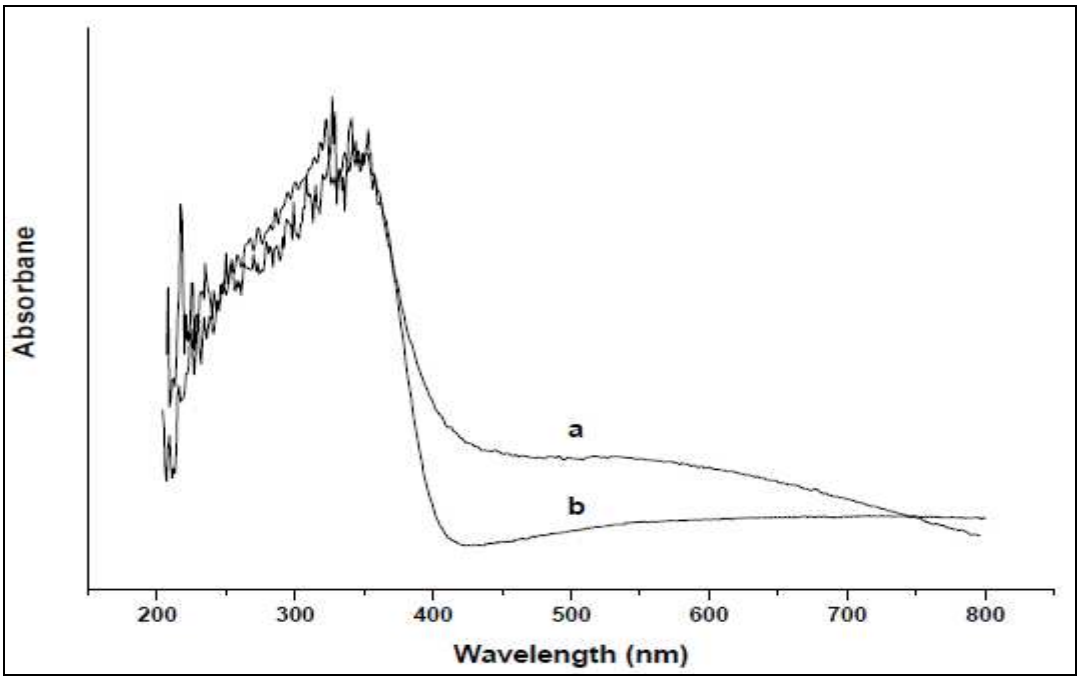

Fig 5.4:UV Vis spectra of (a) Ag(7%) / TiO_2 and (b) TiO_2 (inverse micelle)

5.2.1.3 Photocatalytic Activity

Photocatalytic reduction of CO_2 has been carried out on these materials under ambient conditions and using 77 W Hg lamp as light source. Fig 5.5 compares the methane yield of the metal loaded titania along with their respected pure titania. Fig 5.6. shows the variation of ethanol yield with irradiation time over TiO_2 (inverse micelle) and Ag/TiO_2 .

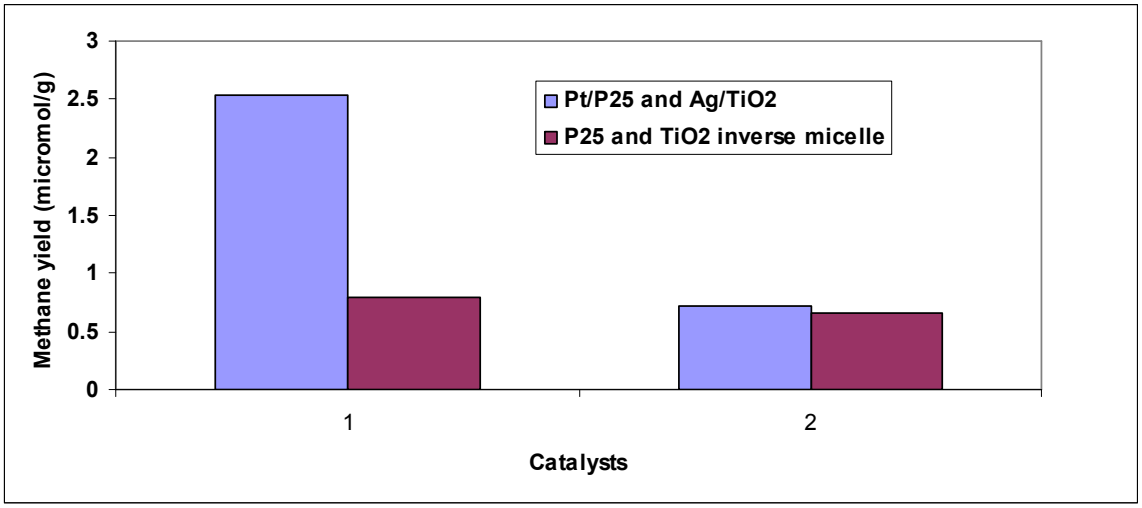

Fig 5.5. Methane yield of the metal loaded titania and the pure titania at 6th hr

Along with methane, traces of acetaldehyde (0.83 μmol/g) was obtained for Pt/P25.

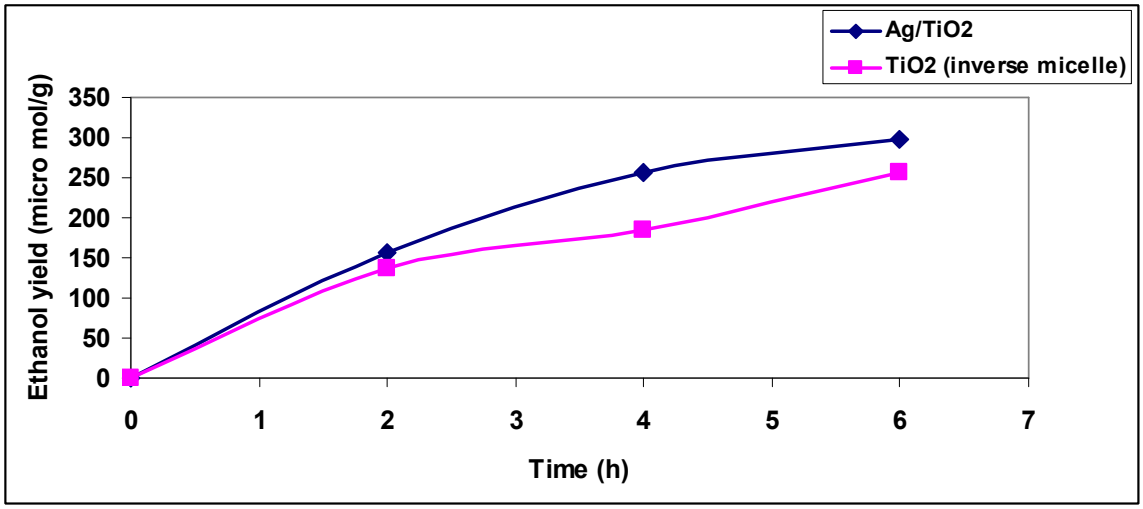

Fig 5.6. Time dependence of ethanol yield over Ag (7 %)/TiO_2 and TiO_2

The difference in crystal phase may be the reason for the selective formation of ethanol in Ag/TiO_2 and TiO_2 (inverse micelle).

From the above figures ,we find that when compared to the pure titania, the metal loaded titania showed improved activity. Methane yield almost increased 3 times in Pt/P25 compared to P25. Whereas, there is negligible increase in methane formation for Ag/

TiO_2 compared to its parent titania (inverse micelle).However ,there is an increase in ethanol formation in Ag / TiO_2

Scheme 5.1 explains the role of metal in metal loaded titania for CO_2 photoreduction

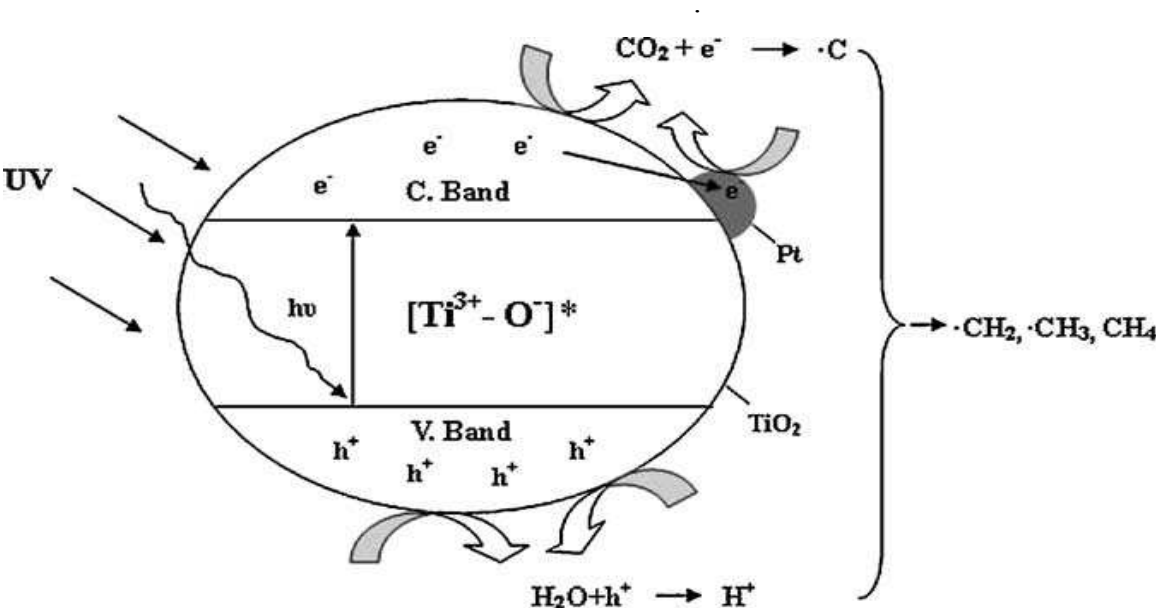

Scheme 5.1. Schematic representation of UV photo-excitation process on Pt/TiO_2 catalyst. (Koci *et al* ,2011)

As irradiated by UV light of suitable wavelength with sufficient photonic energy (hν), photo-generated electron–hole pairs and the charge transfer excited state $[Ti^{3+}–O^-]$* species were created , part of the excited electrons and holes recombined together and radiated out heat or light during the process, while other part that had not recombined would react with the adsorbed reactants on TiO_2 surface. Since Pt-metal had higher work function (Φ_m) than TiO_2 (Φ_s), some electrons transmitted via the Pt-metal and avoided the recombination with holes effectively to extend the life-span of the electron–hole pairs as shown in Scheme 5.1. (Koci *et al* ,2011).

5.2.1.4 Mechanism of photo catalytic reduction of CO_2 with water

Based on the published information on the reaction mechanism, following elementary steps leading to the formation of different products could be envisaged. According to Wu

(2010) the primary process for splitting of water could follow the steps indicated in Scheme 5.2 below.

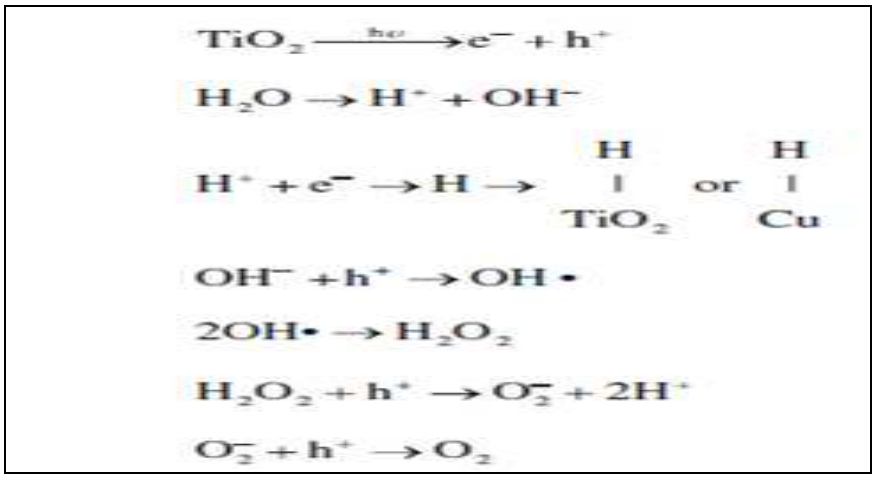

Scheme 5.2. Schematic representation of splitting of water

The second process involving activation of CO_2 and its reduction to various products has been investigated by in-situ FT-IR studies by Wu (2010) and the following pathways are are proposed (Scheme 5.3.)

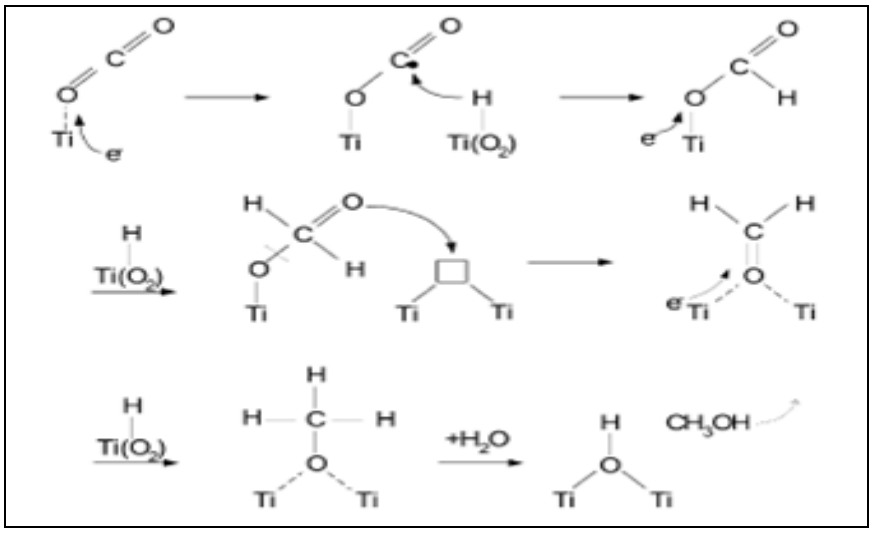

Scheme 5.3. Schematic representation of activation of carbon dioxide

This mechanism entails the formation of methane by further reduction of methanol. However, it is observed that addition of methanol to the reaction medium does not improve the yield of methane (G.R.Dey *et.al*, 2004). Hence a different mechanism

involving the formation of surface carbon radicals, as proposed by Anpo *et al*. (1995), seems to be the more appropriate.

Under this mechanism, the Scheme 5.2 for splitting of water remain unaltered and activation and reduction of CO_2 proceeds through the following steps involving formation of carbon radical ions, as represented by reaction steps below.

$TiO_2 + Hv \longrightarrow e^-(CB) + h^+(VB)$ (5.1)

$H_2O + h^+ \longrightarrow .OH + H^+$ (5.2)

$H^+ + e^- \longrightarrow .H$ (5.3)

$CO_2 + e^- \longrightarrow .CO_2^-$ (5.4)

$.CO_2^- + .H \longrightarrow CO + OH^-$ (5.5)

$CO + e^- \longrightarrow .CO^-$ (5.6)

$.CO^- + H. \longrightarrow .C + OH^-$ (5.7)

$.C + H^+ + e^- \longrightarrow .CH \longrightarrow .CH_2 \longrightarrow .CH_3$ (5.8)

$.CH_3 + H^+ + e^- \longrightarrow CH_4$ (5.9)

$.CH_3 + .OH \longrightarrow CH_3OH$ (5.10)

$.CH_3 + .CH_2 + H^+ \longrightarrow CH_3\text{-}CH_2.$ (5.11)

$CH_3\text{-}CH_2. + OH. \longrightarrow CH_3CH_2OH$ (5.12)

Such a mechanism could also account for the formation of ethanol and is also supported by the observations of carbonaceous deposits on the catalysts. Besides IR & ESR evidence have been reported for the formation of methyl and methoxy radicals on P25 (Dimitrijevic et.al,2011)

Selective formation of ethanol on $BiVO_4$ reported by Liu et.al (2009) can also be explained with the mechanism above. As shown in the Table 5.1. below , rate of formation of ethanol on $BiVO_4$ depends on its crystal structure and the type of radiation used.

Table 5.1.Variation of methanol formation in $BiVO_4$ with crystal structure and lamp intensity (G.Palmisano *et.al*.,2010)

$BiVO_4$	Production rate[a]/ $\mu molh^{-1}$	300 W Xe arc lamp with UV cutoff filter	300 W Xe arc lamp without UV cutoff filter	36 W fluorescent lamp
Monoclinic	Ethanol	21.6	406.6	2.3
	Methanol	0	0	1.8
Tetragonal	Ethanol	1.1	4.9	0.6
	Methanol	0	0	0.6

[a] The rate was determined on the basis of the average production rate after 80 min of irradiation.

In the light of the mechanism above and the observations on $BiVO_4$, formation of ethanol in the case of TiO_2 (inverse micelle) and Ag/TiO_2 needs further investigation.

5.3 STUDIES ON TITANIA COUPLED WITH SEMICONDUCTORS

5.3.1 Results and discussion

5.3.1.1 X-ray diffraction

X-ray diffraction pattern of CuO/P25 is shown in the figure 5.8.It can be seen that for copper loaded TiO_2 , all the characteristic peaks corresponding to P25 were found. CuO diffraction peak appeared near $2\theta = 35.6°$.

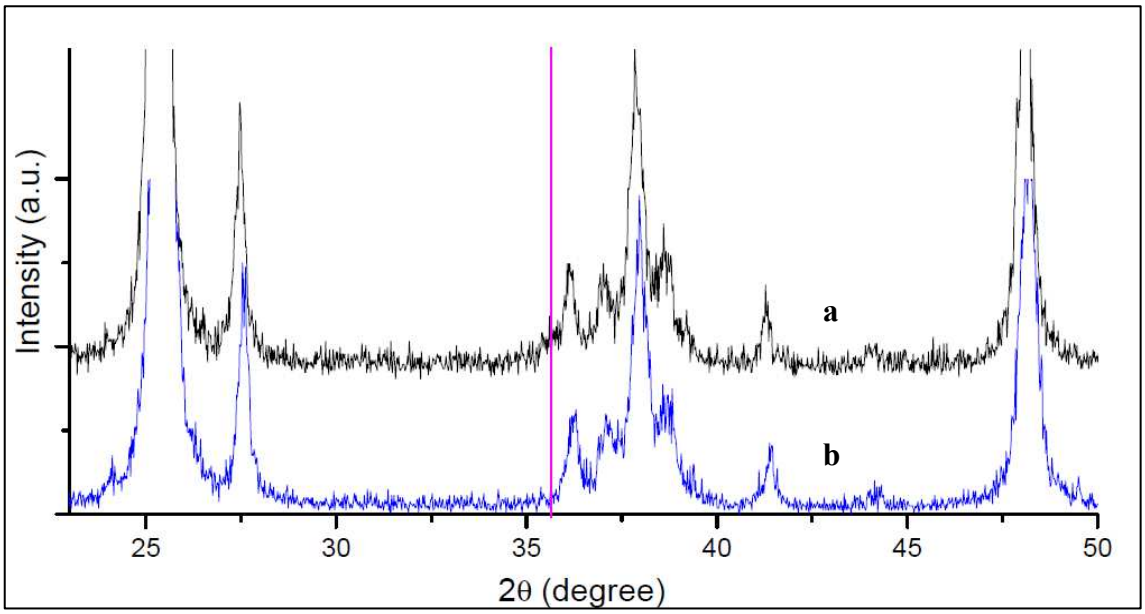

Fig 5.7. X ray diffraction pattern of (a) CuO (3 %) / P25 and (b) P25

X-ray diffraction pattern of NiO / TiO_2 (sol gel) is shown in the fig 5.9. XRD pattern shows that pure anatase is present in NiO (6 %) / TiO_2 and no characteristic peak of NiO appear. Crystallite size of NiO / TiO_2 is found out to be 13.37 nm.

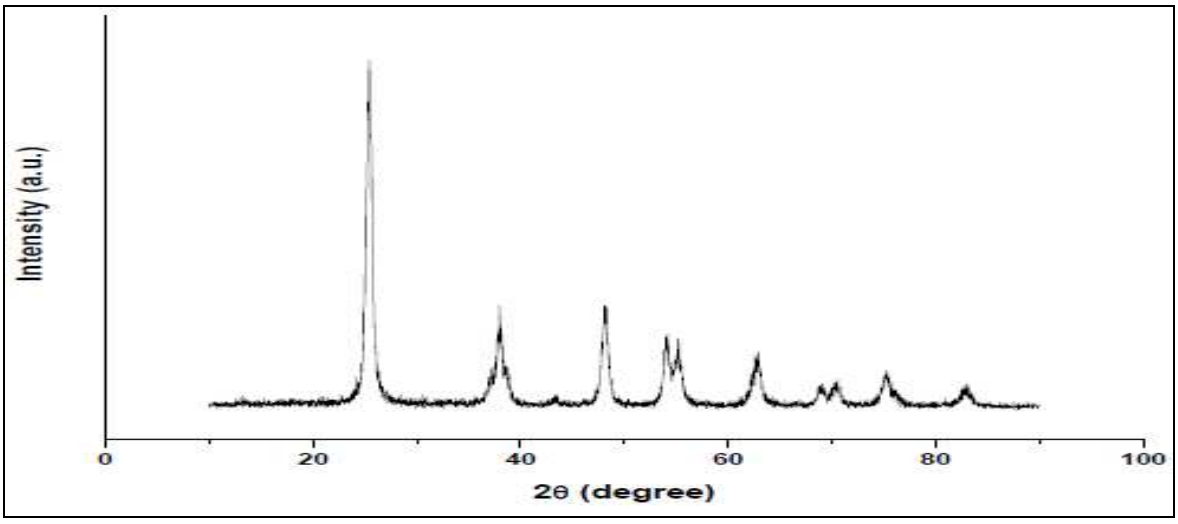

Fig 5.8. X ray diffraction pattern of NiO (6 %)/TiO_2

5.3.1.2 UV -Visible spectra

Fig 5.9. shows the UV-visible absorption spectra of P25 and CuO/P25 .The band gap was estimated by extrapolating the rising segment of the UV spectrum to the abscissa at zero absorption . The band gap of CuO (3 %) / P25 was found out to be 2.82 eV.

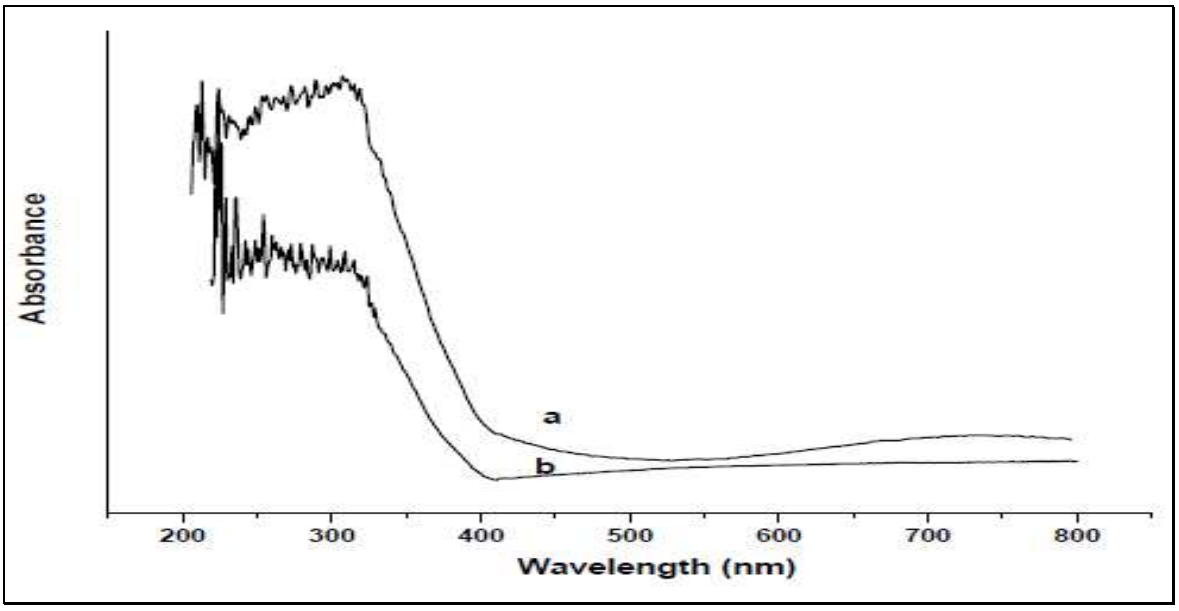

Fig 5.9:UV Vis spectra of (a) CuO(3%) / P25 and (b) P25

Fig 5.10. shows the UV-visible absorption spectra of NiO/TiO_2 (sol gel).

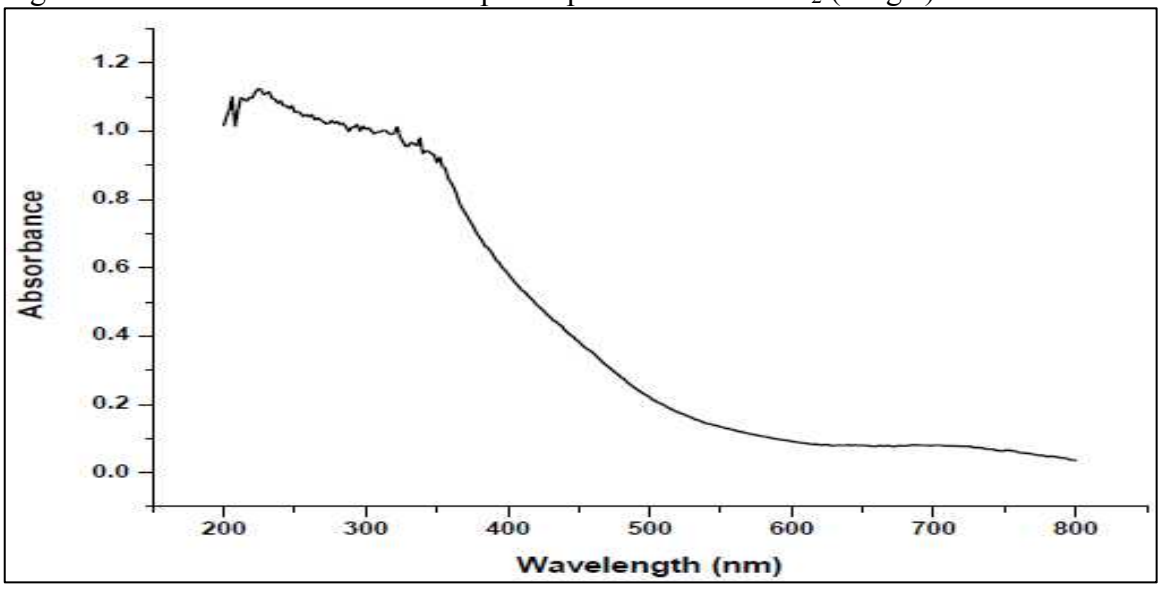

Fig 5.10:UV Vis spectra of NiO/TiO_2

The absorption edge of the NiO/TiO_2 shifts to longer wavelengths .The band gap was found out to be 2.15 eV.

5.3.1.3 TPR studies

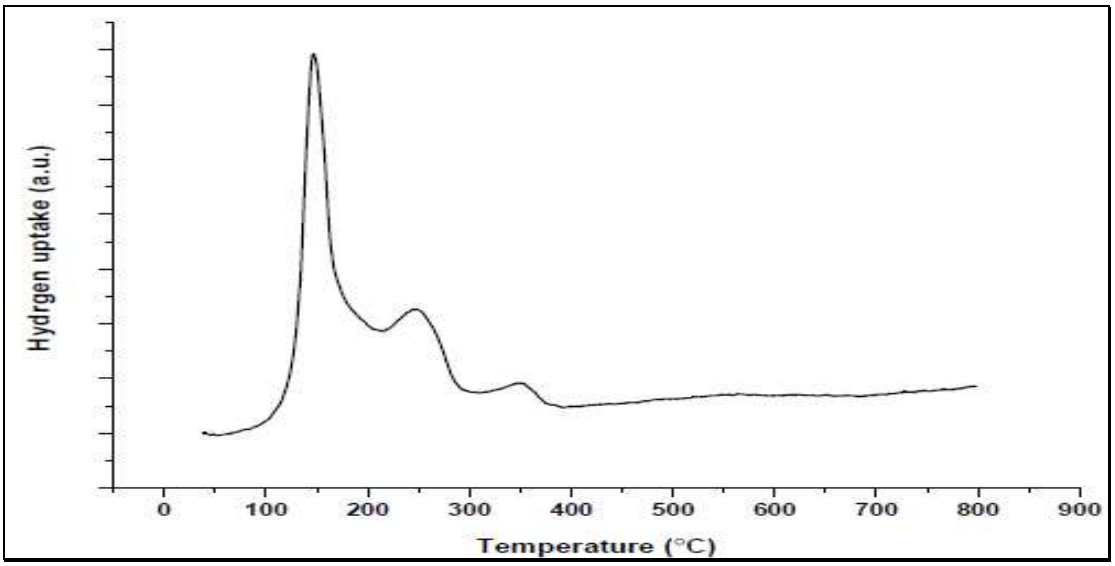

Fig 5.11.TPR profile for the reduction of CuO/P25

TPR result confirmed the presence of CuO in the TiO_2 .

The first sharp peak at 140°C is due to the reduction of dispersed Cu^{2+} and the second peak at 240°C may be due to the reduction of Cu^{2+} that has interacted with the support. The peak at 340°C is possibly due to reduction of titania support (Bond *et al*.,1991). Thus the active phase in this case is Cu^{2+}.

5.3.1.4 Photocatalytic Activity

Photocatalytic reduction of CO_2 has been carried out on these materials under ambient conditions and using 77 W Hg lamp as light source. Fig 5.12 compares the methane yield of the CuO loaded titania along with the pure titania. Fig 5.13. shows the variation of methanol yield with irradiation time over P25 and CuO/P25 .

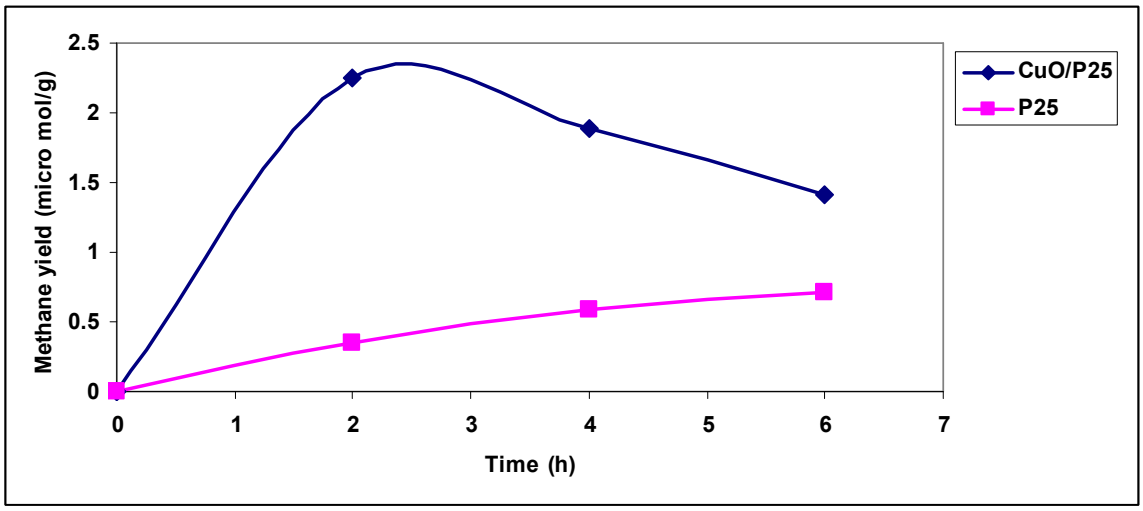

Fig 5.12. Time dependence of methane yield over CuO (3 %)/P25 and P25

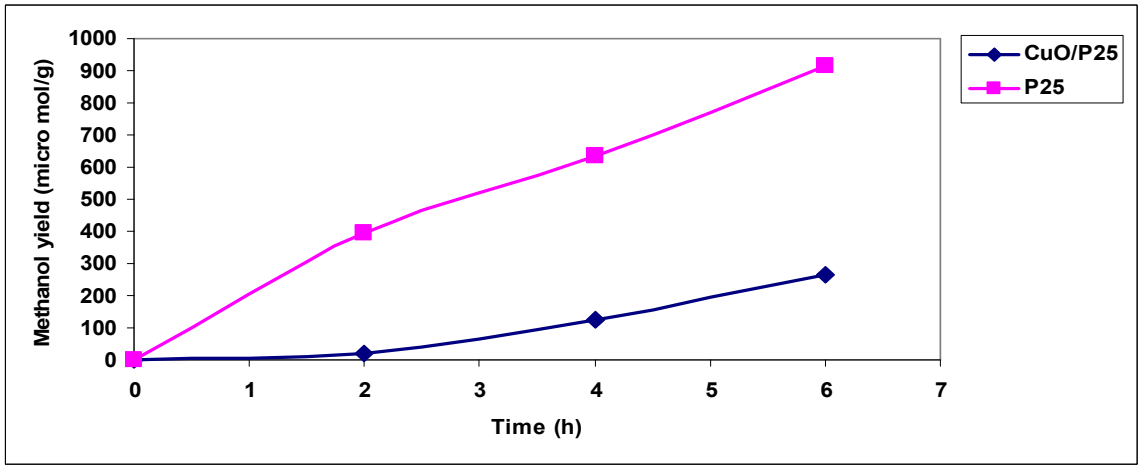

Fig 5.13. Time dependence of methanol yield over CuO (3%) /P25 and P25

Loading CuO on P25 showed enhanced formation of methane.

Fig 5.14 shows the variation of methane yield over NiO(6 %)/TiO_2.

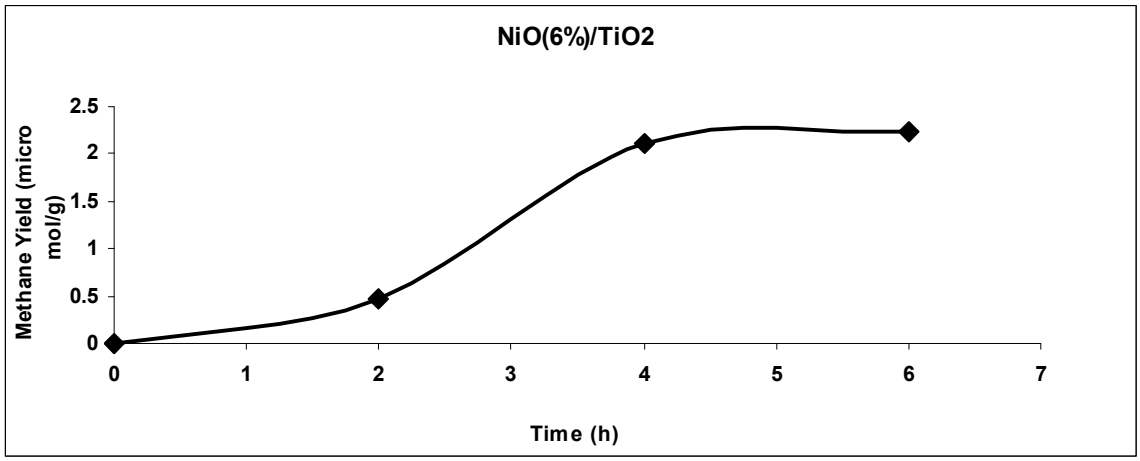

Fig 5.14. Time dependence of methane yield over NiO (6 %)/ TiO_2.

NiO/TiO_2 prepared by improved sol gel method showed methane formation. Fig 5.15. shows the schematic representation of titania coupled semiconductor.

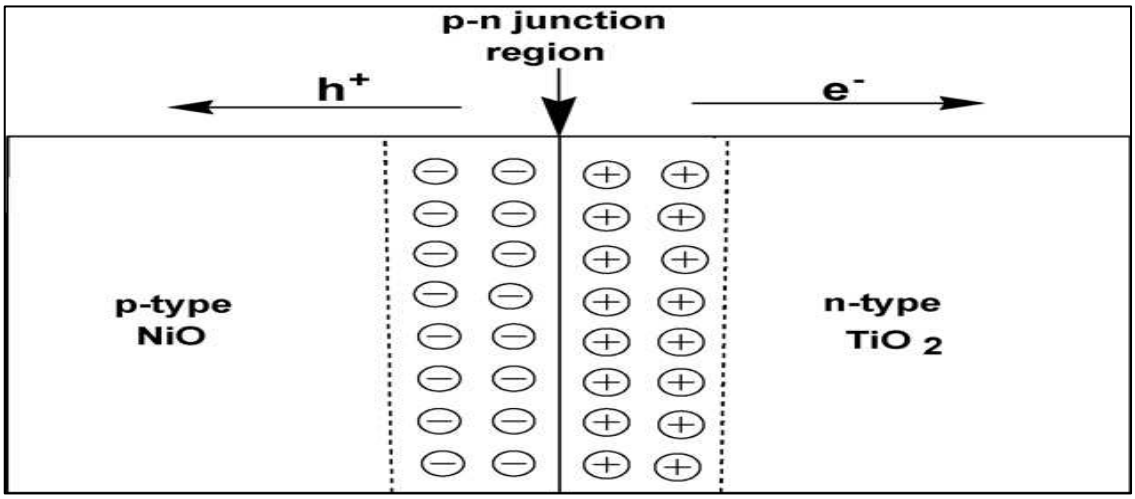

Fig 5.15. Pictorial representation of NiO-TiO_2 heterostructure (Shifu *et al.,*2008)

Under near UV illumination, electron–hole pairs may be created on the n-type semiconductor TiO2 surface, and the photogenerated electron–hole pairs are separated by the inner electric field. The holes flow into the negative field and the electrons move to the positive field. As a result, the photogenerated electrons and holes are separated efficiently, and the photocatalytic activity is enhanced.

Both CuO & NiO coupled titania catalysts show increase in methane formation vis –a vis titania.

CHAPTER 6

INVESTIGATIONS ON Ta & Ti BASED MIXED OXIDES

6.1 La PROMOTED $NaTaO_3$

6.1.1 Introduction

A semiconductor photo catalyst mediating CO_2 reduction and water oxidation needs to absorb light energy, generate electron- hole pairs, spatially separate them, transfer them to redox active species across the interface and minimize electron hole recombination. This requires the semiconductor to have its conduction band electrons at higher energy level compared to the CO_2 reduction potential while the holes in the valence band to be able to oxidize water to O_2. $NaTaO_3$ is one such semionductor satisfying the above requirements. In particular, $NaTaO_3$ with a perovskite structure is most active among alkali metal (Li,Na,K,Rb) tantalates. (Kato et al.,2001)

However, the $NaTaO_3$ photocatalyst gets deactivated with the reaction time during water splitting. It is important to suppress the deactivation and improve the photo catalytic activity. It was reported by Kato *et al* (2003) that NiO/La: $NaTaO_3$ that showed an quantum efficiency of about of 56% at 270 nm. The reason for this high activity is that on substitution of La on $NaTaO_3$ creates a nano step structure. The H_2 evolution site of the edge is effectively separated from the O_2 evolution site of the groove at the surface nanostep structure. At the edges of the reduction sites , water can be efficiently reduced to H_2 on the highly dispersed ultrafine NiO particles. On the other hand, the grooves of the nanostep structure provide the catalytic active sites for O_2 formation accompanied with four-electrons oxidation and the coupling of oxidized intermediate species as shown in Fig 6.1 . This separation is advantageous, especially for water splitting in order to avoid the back reaction.

Teramura *et al* (2010) carried out the Photocatalytic reduction of CO_2 using external H_2 as reductant over $ATaO_3$ photo catalysts [A = Li, Na, K]. The product CO generated strongly depends on the amount of chemisorbed CO_2 in the case of $ATaO_3$ A = Li, Na, K] CO_2 chemisorbed was found out to be 0.2 μmol/g for $NaTaO_3$.

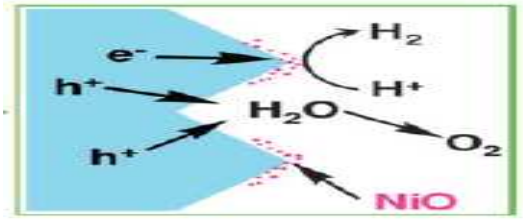

Fig 6.1. Mechanism of water splitting over NiO/La:$NaTaO_3$ photocatalyst. (Kudo *et al.*,2008)

It was observed that NiO/La: $NaTaO_3$ has not been explored for CO_2 photoreduction with water, though it meets required energy level characteristics. Hence this catalyst system was taken up for study.

6.1.2 Results and Discussion

6.1.2.1 X-ray diffraction study

X-ray diffraction patterns of the $NaTaO_3$ prepared by solid state and hydrothermal method are presented in Fig 6.2. All diffraction peaks of $NaTaO_3$ prepared by hydrothermal method can be readily assigned to pure phase $NaTaO_3$ using Joint committee on Powder Diffraction Standards (JCPDS- 25-0863) and no diffraction peaks from the raw material Ta_2O_5 was found. Crystallite size calculated by Scherrer's formula was found out to be 40 nm.

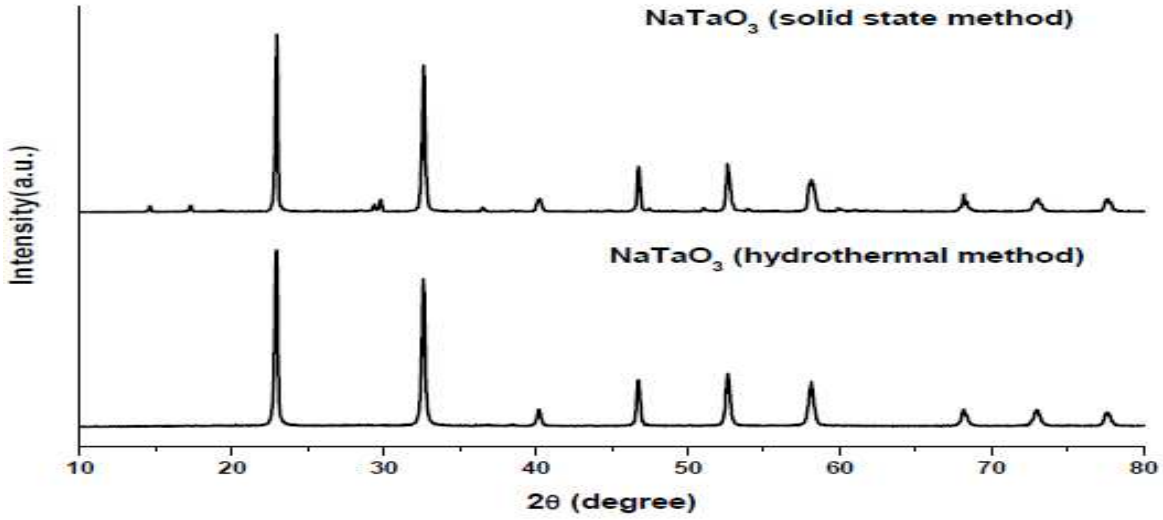

Fig 6.2.XRD pattern of $NaTaO_3$ prepared by solid state and hydrothermal method

However for $NaTaO_3$ prepared by solid state method, peaks due to both pure Na_2CO_3 and Ta_2O_5 were observed. This could be due to incomplete solid state reaction. Therefore for all further studies, sample prepared by hydrothermal method was used.

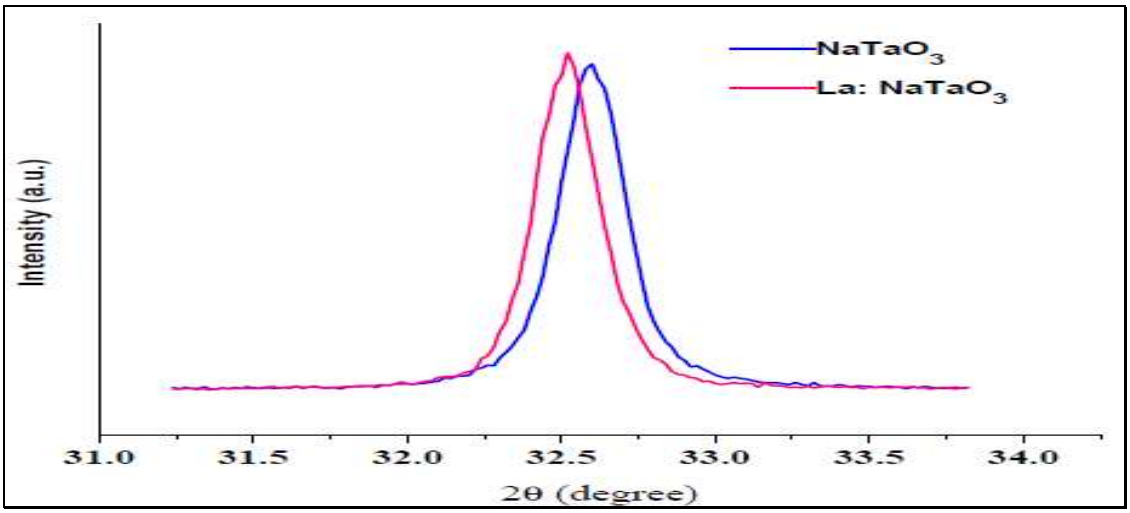

Figure 6.3. X-ray diffraction peaks around 32.5° of $NaTaO_3$ and $NaTaO_3$ substituted with 2% lanthanum

XRD lines of La doped $NaTaO_3$ were slightly shifted to lower angles as reported in the literature. Ionic radii of 12-coordinated La^{3+} (1.36 Å) and Na^+ (1.39 Å) ions are almost the same as each other. In contrast, an ionic radius of the six-coordinated La^{3+} ion (1.032 Å) is remarkably larger than that of the Ta^{5+} ion (0.64 Å). If Ta^{5+} ions which were at the position of B sites in perovskite structures were replaced with La^{3+} ions, a large shift should be observed. Moreover, the diffraction pattern of $La_{0.33}TaO_3$ (the occupation factor of the A site is 0.33) with the perovskite structure similar to $NaTaO_3$ was observed at a lower angle than that of $NaTaO_3$. Therefore, the small shifts to lower angles observed in the diffraction patterns of La:$NaTaO_3$ suggested the substitution of lanthanum ions for sodium ions in the bulk which occupied A sites in perovskite structures (Li *et al*.,2009).

6.1.2.2 UV -Visible spectra

UV -Visible absorption spectra for $NaTaO_3$ and La:$NaTaO_3$ prepared by hydrothermal method is shown in the fig 6.4.

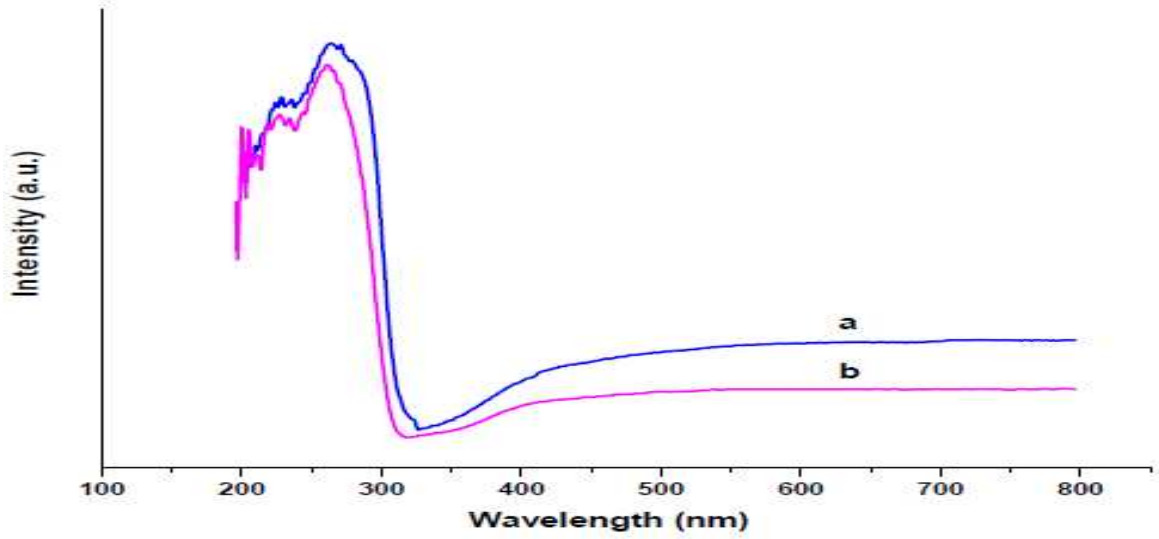

Fig 6.4.UV Visible spectra of a) $NaTaO_3$ and b)La:$NaTaO_3$.

The band gap (from the linear portion of Fig 6.4) was estimated to be 4.1 eV which was 0.2 eV higher than non doped $NaTaO_3$. The estimated bandgap values are close to the values reported in the literature (Li *et al*.,2009). There was a negative shift in conduction on substituting La on $NaTaO_3$.

6.1.2.3 Electron microscopic analysis

a. Scanning electron micrograph

Surface morphology of NiO/La:$NaTaO_3$ has been studied by scanning electron microscopy. The SEM pictures of NiO/ La:$NaTaO_3$ are presented in Fig 6.5. $NaTaO_3$ and La substituted $NaTaO_3$ possess cubic morphology.

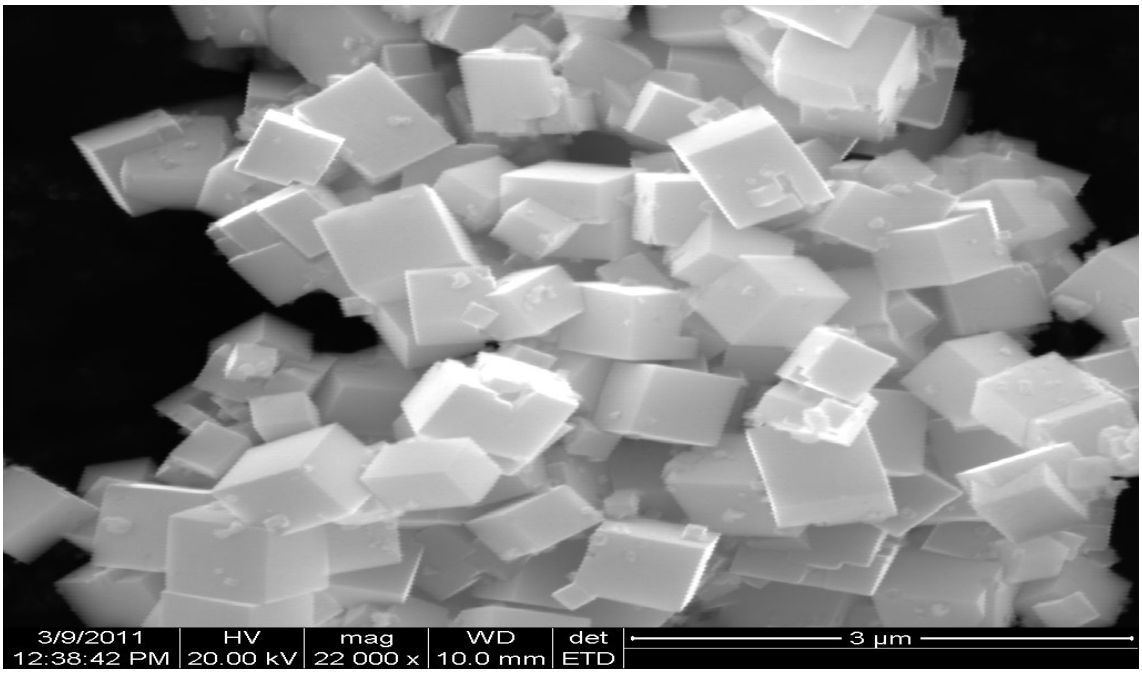

Fig 6.5. SEM photograph of $NiO/La:NaTaO_3$

The corresponding energy dispersive X-ray (EDS) spectrum of the $NiO/La:NaTaO_3$ nanocubes sample shows that it is composed of Na, Ta, La ,Ni and O, no other impurities were detected.

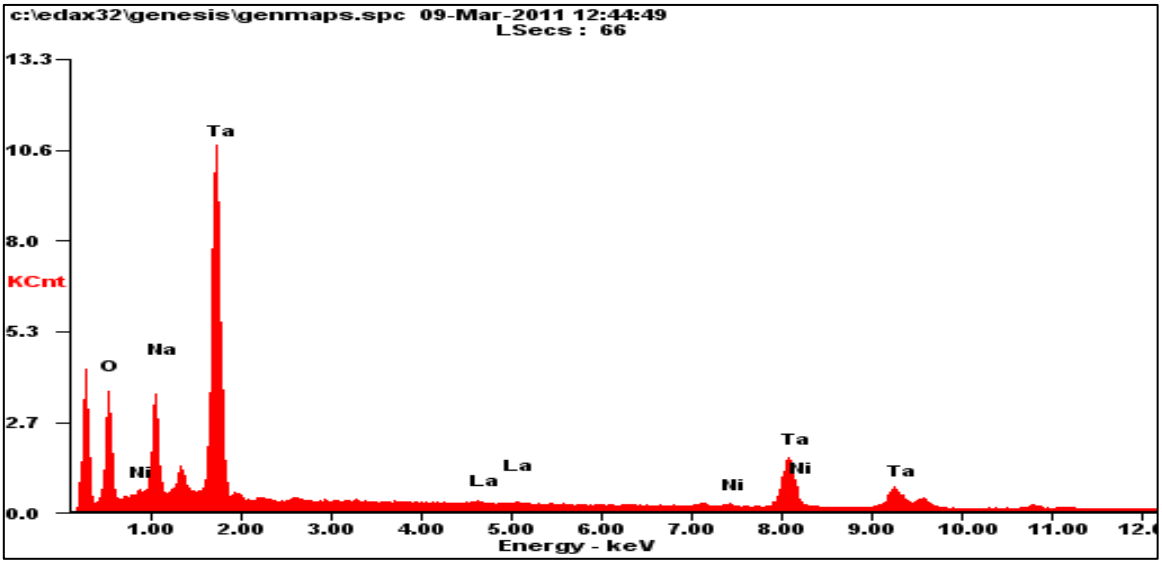

Fig 6.6. EDS spectrum of $NiO/La:NaTaO_3$

b.Transmission electron micrograph

The Transmission electron micrographs of La:$NaTaO_3$ and $NaTaO_3$ are shown in fig 6.7 and fig 6.8. The cube length of La: $NaTaO_3$ varies from 100-300nm. The measured *d* spacing of about 0.389 nm corresponds to the (002) planes of orthorhombic phase $NaTaO_3$.

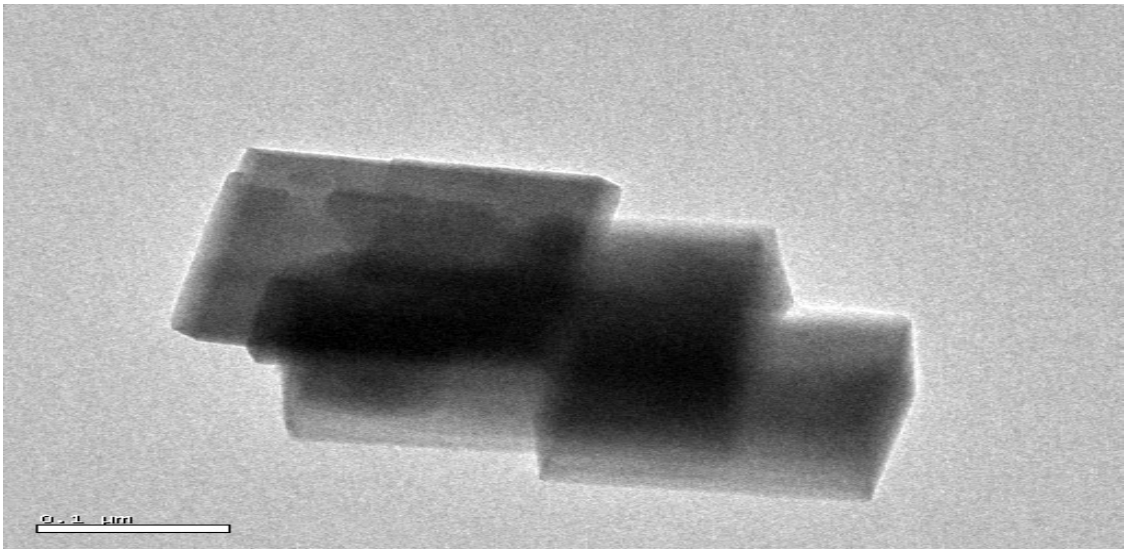

Fig 6.7. TEM image of NiO/ La:$NaTaO_3$

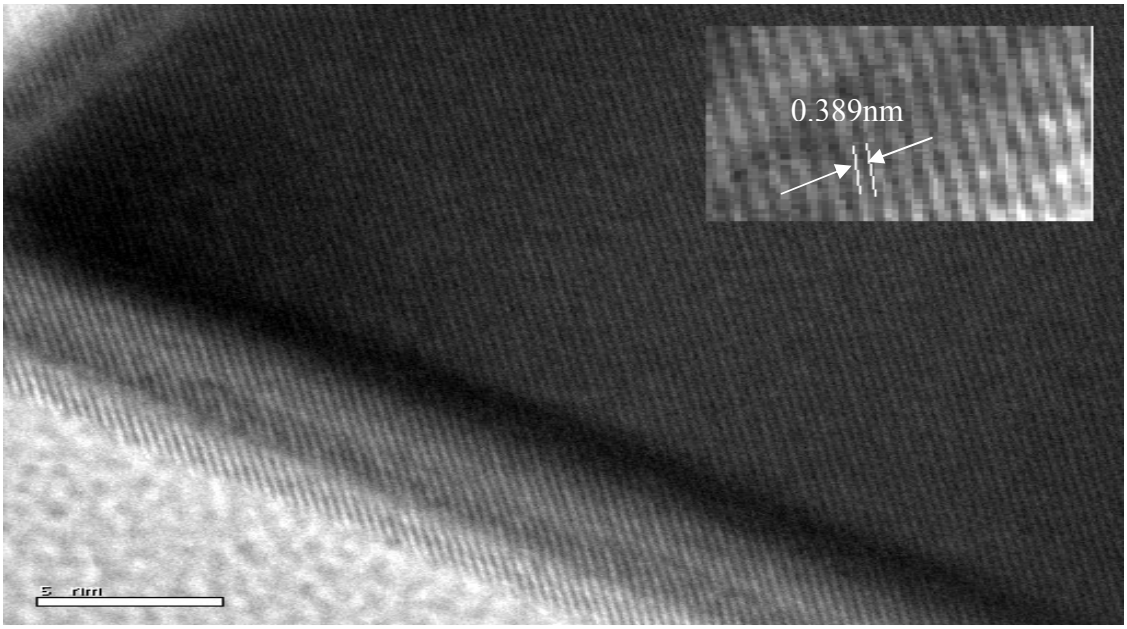

Fig 6.8. TEM image of $NaTaO_3$

6.1.2.4 Photocatalytic Activity

Photocatalytic reduction of CO_2 has been carried out on these materials under ambient conditions and using 77 W Hg lamp as light source. The yield of products is presented in Table 6.1. Fig 6.9. shows the variation of methanol yield with irradiation time over both the catalysts. From the results, it can be seen that the product yield is higher for NiO/La:$NaTaO_3$ than pure $NaTaO_3$.

Table 6.1.Acetone and acetaldehyde yield for $NaTaO_3$ and NiO/La:$NaTaO_3$ at 6^{th}hr.

Product	**NiO/La:$NaTaO_3$**	**$NaTaO_3$**
Acetone	75.33 µmol/g	94.14 µmol/g
Acetaldehyde	25.41 µmol/g	-

Acetone attains maximum yield during 6^{th} hr, whereas acetaldehyde in 4^{th} hr.

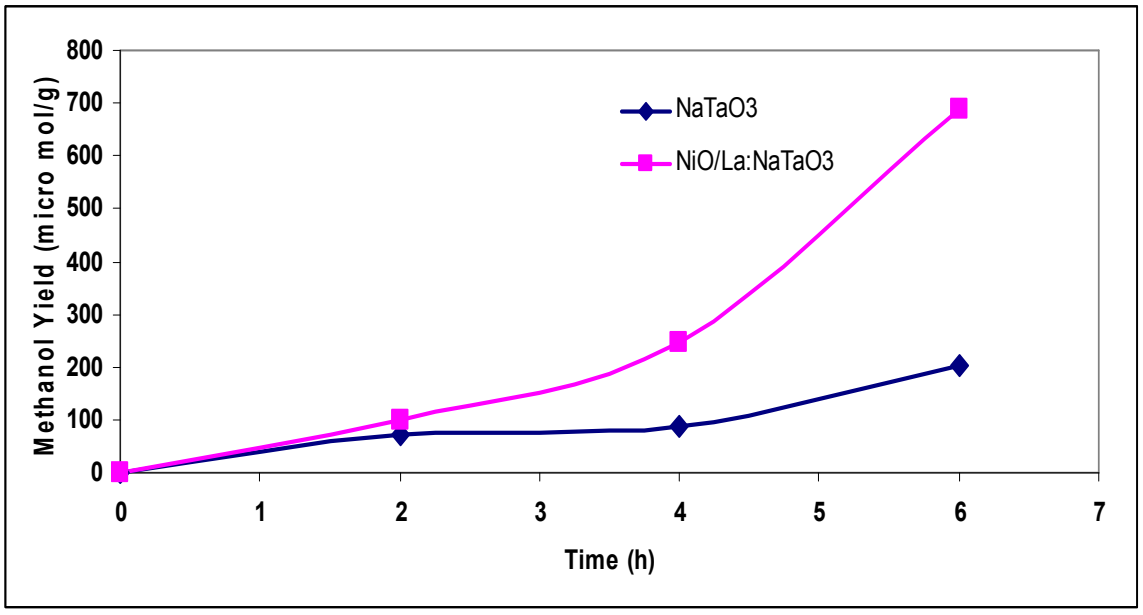

Fig 6.9. Time dependence of methanol yield over $NaTaO_3$ and NiO/La:$NaTaO_3$

As we can see from the plot, the obtained methanol is 6 times greater in NiO/La:$NaTaO_3$ than $NaTaO_3$. The reason for this high activity is as follows.

6.1.2.5 Comparison between $NaTaO_3$ and NiO/La:$NaTaO_3$

The Photocatalytic reaction studies show that NiO/La:$NaTaO_3$ is more active than $NaTaO_3$. However, pure $NaTaO_3$ is itself capable of carrying out CO_2 photo reduction, one of the reason being its ability to chemisorb CO_2 .Also its Conduction band edge is suitable for CO_2 reduction into hydrocarbons. Fig 6.10 presents the band structure of $NaTaO_3$ at pH=0 (Liu *et al*.,2007).Its conduction band edge lies at -1.02 eV.

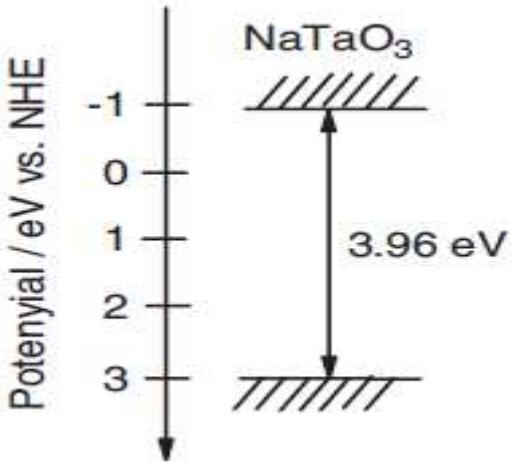

Fig 6.10. Band structure of $NaTaO_3$

Effect of La and NiO

Introduction of Lanthanum ions into the $NaTaO_3$ lattice modifies the conduction band edge, i.e.makes it more negative. Also Lanthanum incorporation creates a surface nano step structure, thereby separating hydrogen and oxygen evolution sites.

When NiO and $NaTaO_3$ are brought into contact, their Fermi levels align, due to the charge transfer phenomenon. In an n-type semiconductor ($NaTaO_3$), a depletion region forms near the junction, as Scheme 6.1 shows. Therefore, under illumination, the n-type $NaTaO_3$ produces a forward-bias voltage that causes electron diffusion across the depletion region to the p-type NiO for H_2 evolution (Scheme 6.2).

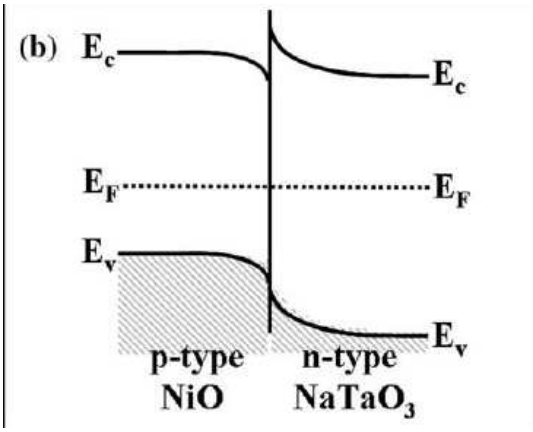

Scheme 6.1. After joining NiO and $NaTaO_3$

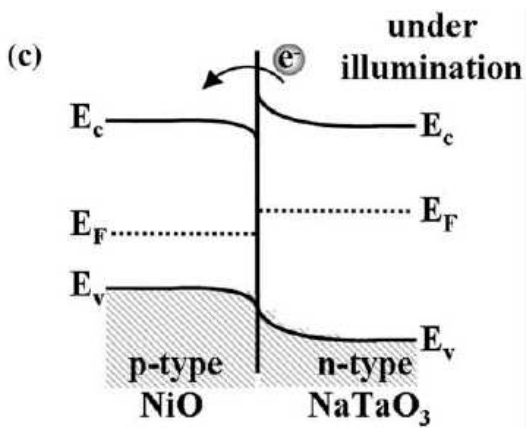

Scheme 6.2. After illumination.

(Hu and Teng ,2010)

All these factors have contributed to a higher yield on NiO/La:$NaTaO_3$.

6.2 STUDIES ON LAYERED PEROVSKITES

6.2.1 Introduction

The interest of these layered perovskites for the photochemical reactions derives from the possibility to use their interlayer space for reaction sites, where electron–hole recombination processes could be retarded by physical separation of electron and hole pairs generated by photo absorption (Centi and Perathoner,2008) .

$La_2Ti_2O_7$ is a member of the (110)-layered Perovskites . It consists of four TiO_6 unit thick slabs that are separated by layers of La^{3+} ions. NiO/Ba-$La_2Ti_2O_7$, a layered perovskite-type oxide has quantum efficiency close to 50% for water splitting in the presence of NaOH . Therefore this catalyst was chosen for CO_2 reduction studies.

$Sr_3Ti_2O_7$ is a member of the (100) – layered perovskites . That is in these materials, slabs of $SrTiO_3$ are cut parallel to the idealised cubic perovskite (100) planes and stacked together , each slab being slightly displaced from the process. The structure of the junction region is identical to that of lamellae of halite (NaCl) structure and so this series can be thought as being composed of intergrowths of varying thicknesses of pervoskite $SrTiO_3$ linked with halite SrO. The flat band potentials of $Sr_3Ti_2O_7$ are favourable for CO_2 photoreduction as well as hydrogen evolution by water spitting. Hence this system was chosen for the study.

6.2.2 Results and discussions

6.2.2.1 X-ray diffraction study

X-ray diffraction pattern of Ba (8%)-$La_2Ti_2O_7$ prepared by solid state method is presented in the fig 6.11.

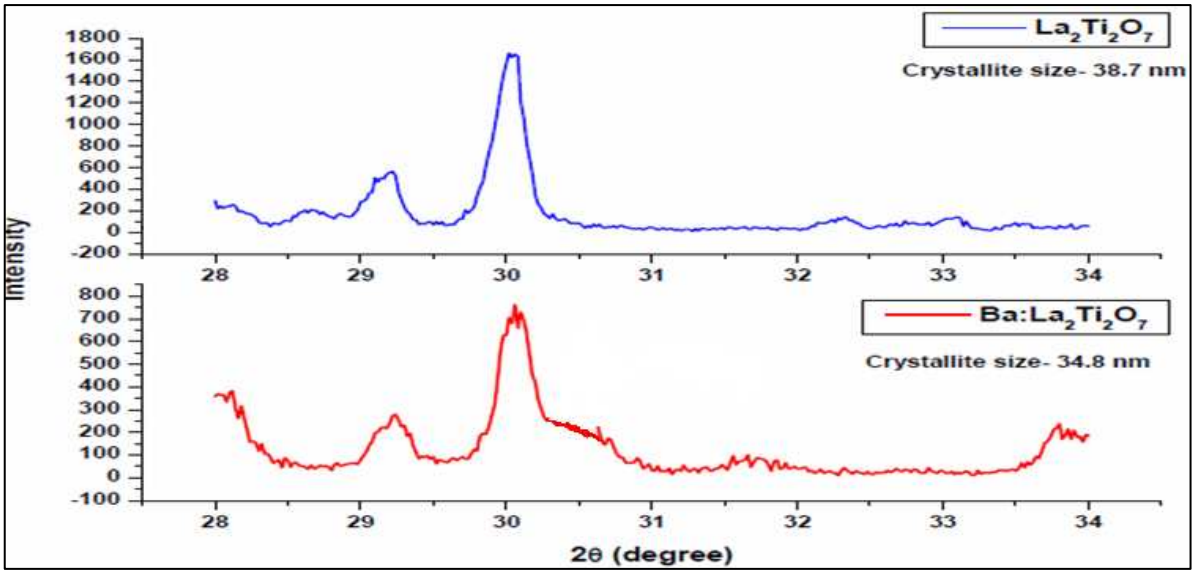

Fig 6.11. X ray Diffraction pattern of $La_2Ti_2O_7$ and Ba (8%)-$La_2Ti_2O_7$

The ionic radii of Ba^{2+} (1.56Å) is greater than La^{3+} (1.30Å).Therefore substitution of Ba^{2+} for La^{3+} leads to the expansion of the $La_2Ti_2O_7$ lattice .Hence the XRD pattern of Ba (8 %)-$La_2Ti_2O_7$ was slightly shifted to lower angles.

The XRD pattern of $Sr_3Ti_2O_7$ prepared by both Polymerised complex and solid state method is shown in the figure 6.12. When compared to solid state method, one could obtain a pure phase of $Sr_3Ti_2O_7$ by polymerized complex method. The standard pattern of $Sr_3T_2O_7$ were taken from JCPDS (card no:78-2479) and compared. All the diffraction lines belonged to $Sr_3Ti_2O_7$. Crystallite size was found to be 55.1 nm.

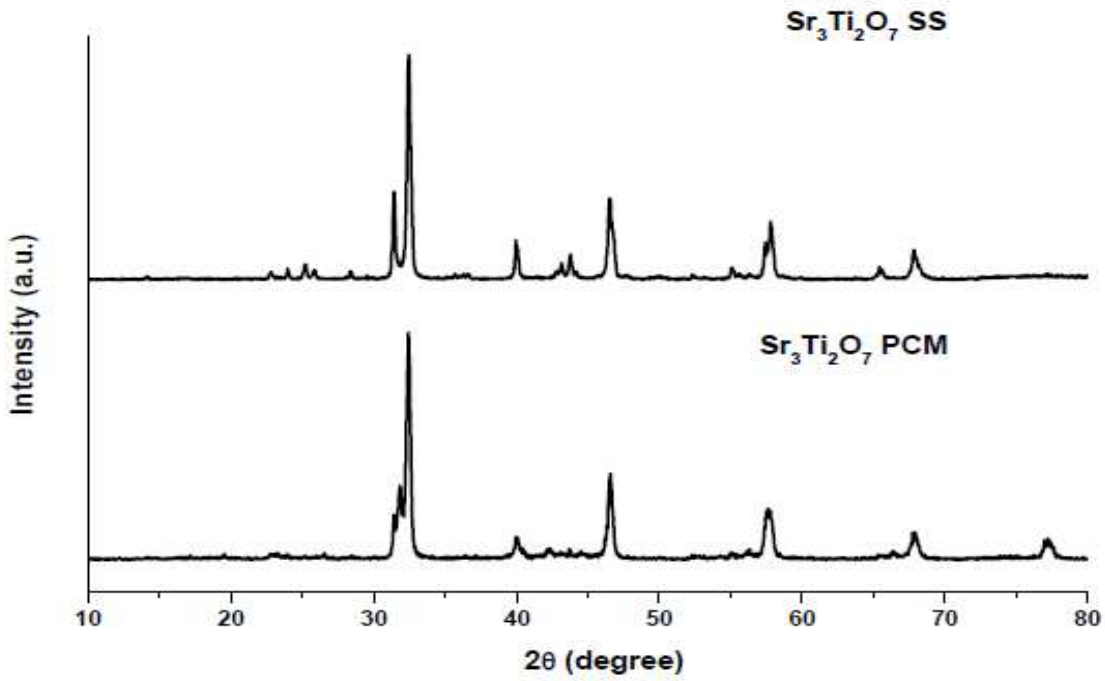

Fig 6.12. X ray diffraction pattern of $Sr_3Ti_2O_7$ prepared by solid state and polymerized complex method.

6.2.2.2 UV -Visible spectra

UV -Visible absorption spectra for Ba:$La_2Ti_2O_7$ is presented in the fig 6.13.

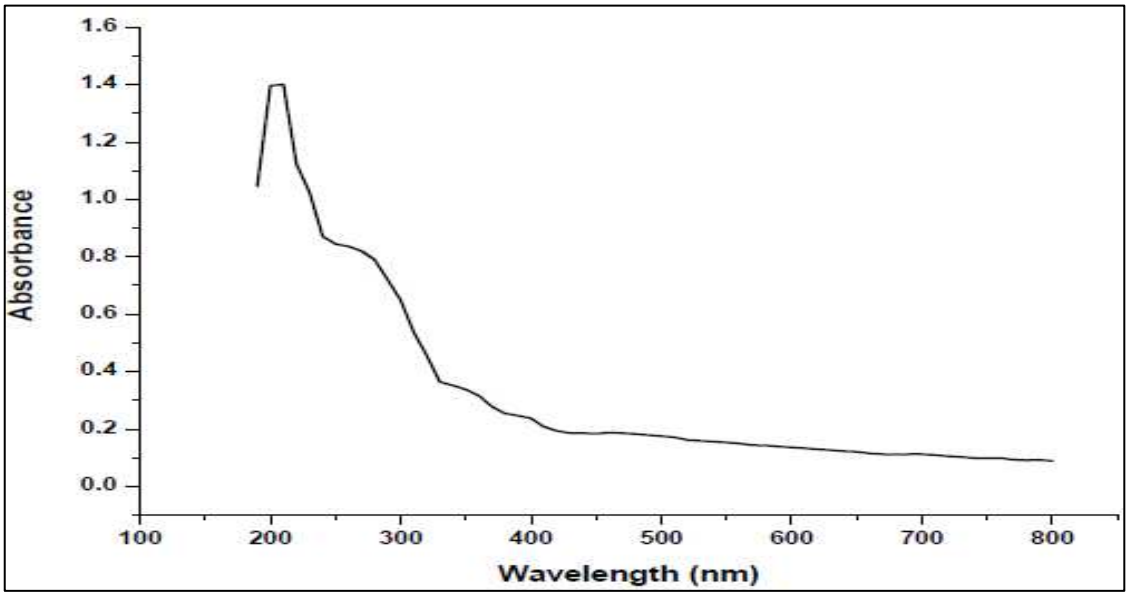

Fig 6.13.UV Visible spectra of Ba:$La_2Ti_2O_7$

The band gap energy of Ba: $La_2Ti_2O_7$ was found to be 3.647 eV .

UV -Visible absorption spectra for $Sr_3Ti_2O_7$ is shown in the fig 6.14.

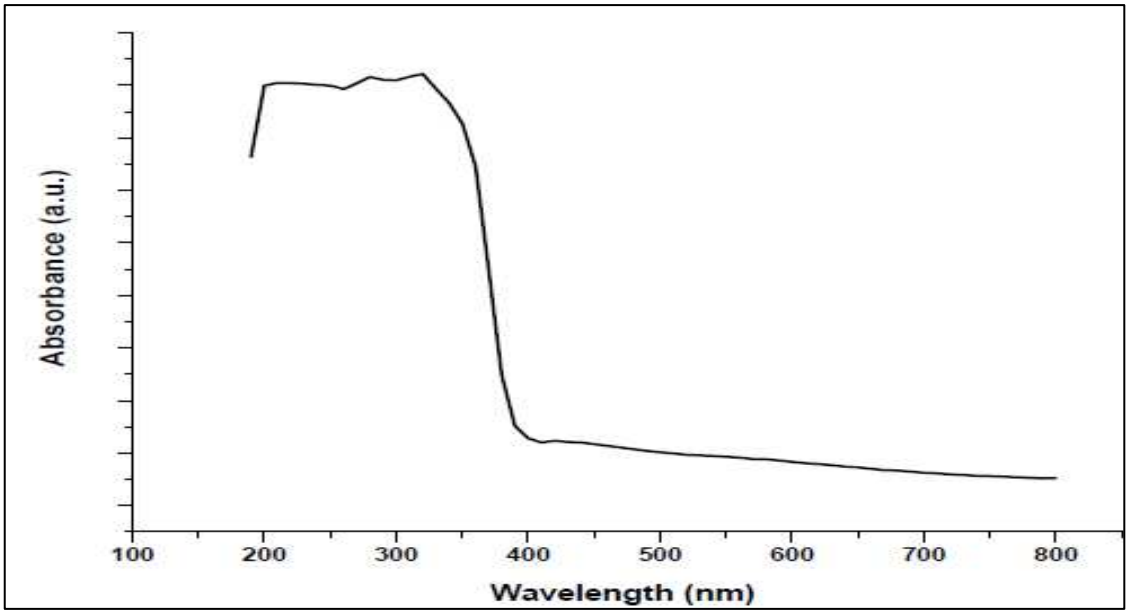

Fig 6.14.UV Visible spectra of $Sr_3Ti_2O_7$

The band gap of the catalyst was estimated to be 3.2eV .

6.2.2.3 Scanning electron micrograph

Surface morphology of NiO/ Ba:$La_2Ti_2O_7$ has been studied by scanning electron microscopy. The SEM pictures of NiO/ Ba:$La_2Ti_2O_7$ are presented in Fig 6.15.

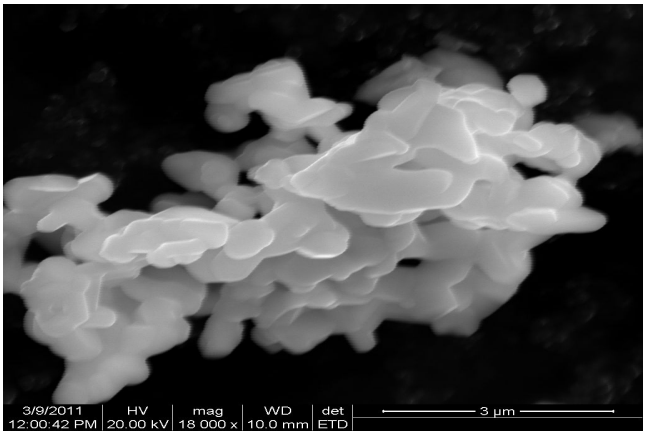

Fig 6.15. SEM photograph of NiO/ Ba:$La_2Ti_2O_7$

6.2.2.4 Photocatalytic Activity

Photocatalytic reduction of CO_2 has been carried out on these materials under ambient conditions and using 77 W Hg lamp as light source. Fig 6.16. shows the variation of methane yield with irradiation time over both the catalysts. The yield of other products are presented in Table 6.2 .

Table 6.2. Acetone , Methanol and acetaldehyde yield for NiO/Ba:$La_2Ti_2O_7$ and $Sr_3Ti_2O_7$ at 6thhr.

Product	**NiO/Ba:$La_2Ti_2O_7$**	**$Sr_3Ti_2O_7$**
acetaldehyde	1.82 µmol/g	21.2
Methanol	-	495.33
Acetone	32.3	-

Methanol yield reaches a maximum of 1064 µmol/g at 4th hour after which it gradually decreases for $Sr_3Ti_2O_7$ catalyst. Where as no methanol was detected for NiO/Ba:$La_2Ti_2O_7$.

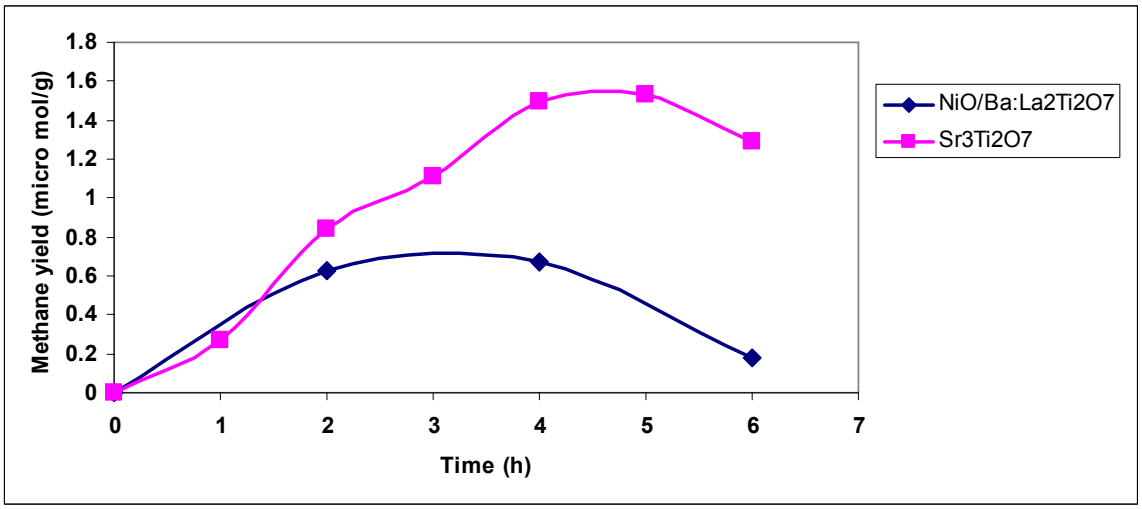

Fig 6.16. Time dependence of methane yield over NiO/Ba:$La_2Ti_2O_7$ and $Sr_3Ti_2O_7$

The distribution of product clearly shows that $Sr_3Ti_2O_7$ is more active than NiO/Ba:$La_2Ti_2O_7$

6.2.2.5 Comparison between $Sr_3Ti_2O_7$ and NiO/Ba:$La_2Ti_2O_7$

Hwang *et al* (2000) observed that (110) layered perovskite $La_2Ti_2O_7$ is more active than (100) layered perovskite $Sr_3Ti_2O_7$.

It was found that the total cation valency of the layered perovskite was the most crucial variable to the high photocatalytic activity. Since the thickness of this layer is inversely proportional to the electron density ,the highly donor-doped perovskite materials would create a narrower depletion layer than perovskites of the normal valency. Then, band bending would take place over this depletion layer with a narrower width or become more drastic .This would result in fewer electron hole recombination.

Further ,the substitution of Barium into the $La_2Ti_2O_7$ lattice leads to the following effect (Kim *et al*.,2005). The role of Barium was to increase the hydroxyl concentration on the surface of $La_2Ti_2O_7$ during the reaction. The surface hydroxyl group can then effectively act as the hole scavenger. Also modification of catalyst surface of layered perovskite with hydroxyl group (OH^-) could enhance its photocatalytic activity by changing the property of interface between catalyst and electrolyte.

However, from Table 6.2 and Fig 6.16 we find that $Sr_3Ti_2O_7$ is more active than NiO/Ba: $La_2Ti_2O_7$ .This may be due to their difference in the band gap. The band gap of NiO/Ba: $La_2Ti_2O_7$ is 3.65 eV whereas ,for $Sr_3Ti_2O_7$ it is 3.2 eV.

It is well known that the light wavelength influences the yield of CO_2 photo catalytic reduction products (Koci *et al*.,2008).The Hg lamp used for the reaction has the maximum intensity at 360 nm. Irradiation using shorter wavelength would be more effective for NiO/Ba: $La_2Ti_2O_7$ due its band gap.

CHAPTER 7

SUMMARY & CONCLUSIONS

Photo catalytic reduction of carbon dioxide with water to yield fuels/chemicals (methane, methanol, etc.,) on semiconductor oxide catalyst surfaces has the potential to become a viable and sustainable alternative energy source to fossil fuels. However, it has to cross several hurdles since it involves the activation of two thermodynamically most stable molecules, CO_2 and water and simultaneous conversions through complex multi-electron transfer steps. Hence achieving desired product selectivity is a serious challenge.

The process involves two major steps, spitting of water to yield hydrogen which in turn helps in the reduction of carbon dioxide to different hydrocarbon products in the second step. Design of effective catalysts for such a complex process holds the key for the viability of the process.

The objective of the current investigation is to explore new catalyst formulations that can improve hydrocarbon yields from CO_2 and water via photo activation.

Ideal catalysts are expected to display maximum efficiency towards solar energy absorption and possess requisite band energy level characteristics to drive the redox reactions. Functionally, the catalysts should have valence band energy level suitable for splitting of water to generate hydrogen, which is the primary step.The second and the most crucial step is the reduction of CO_2 to hydrocarbons, which requires the energy level of the conduction band to be more negative with respect to reduction potential for CO_2.

With these guiding principles in mind, the thesis focusses on the following aspects for investigation,

- Comparison of the performance of two commercial titania samples (P-25 & HOMBIKAT-UV-100) and two other titania samples prepared (by solgel methods- controlled by hydrolysis in acid medium and reverse micelle) in the laboratory
- Effect of metal loading, as revealed by loading of Pt & Ag
- Effect of using CuO & NiO as coupled semi-conductors with TiO_2
- Preparation of $NaTaO_3$ and NiO/La:$NaTaO_3$ and comparison of activities for CO_2 photo reduction.

- Preparation of layered titanates, $Sr_3Ti_2O_7$ and NiO/Ba:$La_2Ti_2O_7$ and to study the ability of these systems to reduce CO_2

Amongst the catalyst systems chosen for study, $NaTaO_3$, $Sr_3Ti_2O_7$ & $La_2Ti_2O_7$ are known for their activity for photocatalytic splitting of water, but are being explored for the first time towards CO_2 reduction with water. These systems have been chosen based on their band energy level characteristics.

Besides the conventional catalyst preparation methods (wet chemical & solid state reactions) and sol-gel techniques, hydrothermal synthesis (for $NaTaO_3$) and polymer complex methods (for $Sr_3Ti_2O_7$) have been adopted to obtain catalyst samples with desired characteristics.

All the catalysts prepared have undergone comprehensive characterization by XRD (for phase identification & crystallite size) UV-Visible DRS (for band gap), and surface area, temperature programmed reduction, SEM, TEM &EDS, wherever needed.

Catalysts have been evaluated for photo catalytic reduction of CO_2 with water, by dispersing 0.4 g of catalyst in 400 ml of 0.2 M aqueous NaOH using Hg lamp with 77 Watt power, covering the wavelength range 300-700 nm.

Several hydrocarbon products, methane, ethane, methanol, ethanol, formaldehyde, acetaldehyde and acetone have been identified, with methane, methanol and ethanol being the major products.

Amongst the four titania samples investigated, P-25 shows maximum activity in terms of methane and methanol formation. Hombikat-UV-100, in spite of its high surafce area and surface hydroxyl concentration, is relatively less active. P-25, being a anatase- rutile mixed phase, with unique interspacing of valance band and conductance band enegry levels, results in effective charge carrier separation and hence improved activity.

Amongst the two titania samples prepared by sol-gel routes, the sample via inverse micelle formation, shows good activity with ethanol as major product, at the expense of methanol. Further detailed catalyst characterization and evaluation studies are needed to rationalize this observation, in the light of the report that $BiVO_4$ selectively forms ethanol and the yield depends the crystal structure of the catalyst and the wavelength of the radiation used.

In the case of metal loaded titania, Pt/P-25 shows increase in methane formation and the activity (in terms of micro moles of methane formed per gram of catalyst) is close to the value reported in literature (up to six hours on stream time). Silver impreganted on titania (reverse micelle) also exhibits unique behaviour, with ethanol being major product besides methane. Incorporation of silver increases the activity

Both CuO & NiO effectively act as coupled semi-conductors in conjunction with titania and exhibit increase in activity vis-a vis titania.

Results on $NaTaO_3$, $Sr_3Ti_2O_7$ and $La_2Ti_2O_7$ indicate that these mixed oxide systems have good potential to become effective catalyst systems for CO_2 photo reduction when coupled with suitable co-catalysts. La doped and NiO promoted $NaTaO_3$ exhibits increase in methane formation and better stability. Further improvements could be expected with the addition of more effective co-catalysts.

$La_2Ti_2O_7$ is relatively less active compared to strontium titanate. Preparation of La titanate by soft chemistry routes is to be explored so that we can get phase-pure material with higher surafce area.

In conclusion, the investigation has opened up new avenues for exploration on catalysts for CO_2 photo reduction. Choice of catalyst preparation methods, crystal structure, particle size, band energy characteristics of the catalyst and the wavelength of the radiation are the major factors that influence the activity and product

selectivity. Titania based catalysts, with suitable metal /metal oxide as co-catalysts still hold promise as one of the potential sytems for further investigation.

Mixed metal oxide catalysts, especially alkali metal tantalates, & alkaline earth and rare earth metal layered titanates constitute an interesting array of catalysts which are worth further invetigation as catalysts for CO_2 photo reduction.

REFERENCES

1. **Anpo, M., H. Yamashita, Y. Ichihashi,** and **S. Ehara,** (1995) Photocatalytic reduction of CO_2 with water on various Titanium Oxide catalysts. *Journal of Electroanalytical Chemistry*, **396** ,21-26.

2. **Anpo, M.,** and **K. Chiba,** (1992) Photocatalytic Reduction of CO_2 on Anchored Titanium-Oxide Catalysts. *Journal of Molecular Cataysis*, ***74*,** 207–212.

3. **Adachi, K., K. Ohta,** and **T. Mijuma**,(1994) Photocatalytic Reduction of Carbon-Dioxide to Hydrocarbon Using Copper-Loaded Titanium-Dioxide. *Solar Energy,* **53**, 187–190.

4. **Anpo, M., H. Yamashita, Y. Ichihashi, Y. Fujii,** and **M. Honda**,(1998) Photocatalytic Reduction of CO_2 with H_2O on Titanium Oxides Anchored within Micropores of Zeolites: Effects of the Structure of the Active Sites and the Addition of Pt. *Journal of Physical Chemistry. B*, **101**, 2632–2636.

5. **Ahmed, N., Y. Shibata , T. Taniguchi,** and **Y. Izumi (**2011**),** Photocatalytic conversion of carbon dioxide into methanol using zinc–copper–M(III) (M = aluminum, gallium) layered double hydroxides. *Journal of catalysis* doi:10.1016/j.jcat.2011.01.004.

6. **Brus L.,** (1986) Electronic Wave Functions in Semiconductor Clusters: Experiment and Theory. *Journal of Physical Chem*istry, **90,** 2555-2560.

7. **Bond, G. C., N. Stephen , Namijo** and **J. S. Wakeman** (1991) Thermal analysis of catalyst precursors Part 2. Influence of support and metal precursor on the reducibility of copper catalysts. *Journal of Molecular Catalysis,* **64**, 305-319.

8. **Carneiro, J. T., T. J. Savenije, J. A. Moulijn,** and **G. Mul (**2011) How Phase Composition Influences Optoelectronic and Photocatalytic Properties of TiO_2 *Journal of Physical Chemistry C,* **115**, 2211–2217.

9. **Centi, G.,** and **S. Perathoner** (2008) Catalysis by layered materials: A review *Microporous and Mesoporous Materials*, **107**, 3–15.

10. **Deak, P., B. Aradi,** and **T. Frauenheim** (2011) Band Lineup and Charge Carrier Separation in Mixed Rutile-Anatase Systems. *Journal of Physical Chemistry C*, **115**, 3443–3446.

11. **Dey G. R.,** (2007) Chemical Reduction of CO_2 to Different Products during Photo Catalytic Reaction on TiO_2 under Diverse Conditions: an Overview *Journal of Natural Gas Chemistry,* **16,** 217–226.

12. **Demeestere, K., J. Dewulf** and **H. V.** and **Langenhove** ,(2007) Heterogeneous Photocatalysis as an Advanced Oxidation Process for the Abatement of Chlorinated, Monocyclic Aromatic and Sulfurous Volatile Organic Compounds in Air: State of the Art**.** *Critical Reviews in Environmental Science and Technology*, **37,** 489-538.

13**. Dimitrijevic, N. M., B. K. Vijayan, O. G. Poluektov, T. Rajh, K. A. Gray, H. He,** and **P. Zapol** (2011), Role of Water and Carbonates in Photocatalytic Transformation of CO_2 to CH_4 on Titania. *American Chemical Society* 133, 3964–3971

14. **Fan, J., E-Z. Liu, L. Tian, X-Y. Hu, Qi He,** and **T. Sun,**(2010) Study on Synergistic Effect of N and Ni^{2+} on Nano Titania in Photocatalytic Reduction of CO_2 . *American Society of Civil Engineers* doi:10.1061/(ASCE)EE.1943-7870.0000311.

15. **Fujishimaa, A., X. Zhang, Donald,** and **A. Tryk** (2007) Heterogeneous photocatalysis: Fromwater photolysis to applications in environmental cleanup. *International Journal of Hydrogen Energy*, **32,** 2664 – 2672.

16. **Guan, G., T. Kida,** and **A. Yoshida,** (2003) Reduction of Carbon Dioxide with Water under Concentrated Sunlight Using Photocatalyst Combined with Fe-Based Catalyst. *Applied Catalysis, B*, **41**, 387–396.

17. **Guan, G., T. Kida, T. Harada, M. Isayama,** and **A. Yoshida** (2003) Photoreduction of carbon dioxide with water over $K_2Ti_6O_{13}$ Photocatalyst combined with Cu/ZnO catalyst under concentrated sunlight. *Applied Catalysis A: General*, **249,** 11–18.

18. **Guan, G., T. Kida, T. Ma, K. Kimura, E. Abe** and **A. Yoshida,** (2003) Reduction of aqueous CO_2 at ambient temperature using zero-valent iron-based composites. *Green Chemistry*, **5**, 630–634.

19. **Hwang, D.W., H. G. Kim, J. Kim, K. Y. Cha, Y. G. Kim**, and **J. S. Lee** (2000) Photocatalytic Water Splitting over Highly Donor-Doped (110) Layered Perovskites. *Journal of Catalysis*, **193,** 40–48.

20. **Hu, C-C.,** and **H. Teng,** (2010) Structural features of p-type semiconducting NiO as a co-catalyst for Photocatalytic water splitting. *Journal of Catalysis*, **272,** 1–8.

21. **Halmann, M., M. Ulman,** and **B. A. Blajeni,** (1983) Photochemical Solar Collector for the Photoassisted Reduction of Aqueous Carbon-Dioxide. *Solar Energy*, **31**, 429–431.

22. **Halmann, M., V. Katzir, E. Borgarello** and **J. Kiwi** (1984) Photoassisted Carbon dioxide Reduction on Aqueous Suspensions of Titanium Dioxide. *Solar Energy Materials,* **10,** 85-91.

23. **Hoffmann, M., R., S. T. Martin, W. Choi,** and **D. W. Bahnemann** (1995**)** Environmental Applications of Semiconductor Photocatalysis. *Chemical Reviews,* **95**, 69-96.

24. **Hashimoto K., H. Irie** and **A. Fujishima** (2005) TiO_2 Photocatalysis: A Historical Overview and Future Prospects. *Japanese Journal of Applied Physics* **44**, 8269–8285.

25. **Inoue, T., A. Fujishima, S. Konishi,** and **Honda, K.,**(1979) Photoelectrocatalytic Reduction of Carbon-Dioxide in Aqueous Suspensions of Semiconductor Powders. *Nature*, **277**, 637–638.

26. **Indrakanti, V. P., J. D. Kubickib** and **H. H. Schobert** (2009) A Photoinduced activation of CO_2 on Ti-based heterogeneous catalysts: Current state, chemical physics-based insights and outlook. *Energy Environmental Science*, **2,** 745–758.

27. **Jeong, H., T. Kim, D. Kim,** and **K. Kim** (2006) Hydrogen production by the Photocatalytic overallwater splitting on $NiO/Sr_3Ti_2O_7$: Effect of preparation method. *International Journal of Hydrogen Energy,* **31,** 1142 – 1146.

28. **Kočí, K., L. Obalová,** and **Z. Lacný** (2008) Photocatalytic reduction of CO_2 over TiO_2 based catalysts. *Chemical Papers*, **62,** 1–9.

29. **Kaneco, S., H. Kurimoto, K. Ohta, T. Mizuno,** and **Akira**,(1997) Photocatalytic reduction of CO_2 using TiO_2 powders in liquid CO_2 medium. *Journal of Photochemistry and Photobiology A: Chemistry* , **109**, 59-63.

30. **Kocí, K., MartinReli, O. Kozák, Z. Lacny, DanielaPlachá, PetrPraus,** and **LucieObalov** (2010) Influence of reactor geometry on the yield of CO_2 Photocatalytic reduction. *Catalysis Today* doi:10.1016/j.cattod.2010.12.054

31. **Koci .K., K. Mateju, L. Obalova, S. Krejcikova, Z. Lacny, D. Placha, L. Capek, A. Hospodkova,** and **O. Solcova**,(2010) Effect of silver doping on the TiO_2 for Photocatalytic reduction of CO_2. *Applied Catalysis B: Environmental*, **96,** 239–244.

32. **Kohno, Y., H. Hayashi, S. Takenaka, T. Tanaka, T. Funabiki,** and **S. Yoshida,** (1999) Photocatalytic reaction of H_2O+CO_2 over pure and doped Rh/TiO_2. *Journal of Photochemistry and Photobiology A: Chemistry,* **126,** 117-123.

33. **Ku, Y., W-H Lee,** and **W-Y Wang,** (2004) Photocatalytic reduction of carbonate in aqueous solution by UV/TiO_2 process. *Journal of Molecular Catalysis A: Chemical,* **212,** 191–196.

34. **Kanemoto, M., T. Shiragami, C. Pac,** and **S. Yanagida** (1992) Effective Photoreduction of Carbon Dioxide Catalyzed by ZnS Quantum Crystallites with

Low Density of Surface Defects. *Journal of Physical Chemistry C*, **96,** 3521-3526.

35. **Kato, H., K. Asakura**, and **A. Kudo,** (2003) Highly Efficient Water Splitting into H_2 and O_2 over Lanthanum-Doped $NaTaO_3$ Photocatalysts with High Crystallinity and Surface Nanostructure. *Journal of American Chemical Society,* **125,** 3082-3089.

36. **Kima, J., D. W. Hwanga, H. G. Kim, S. W. Bae, J. S. Leea, W. Lib,** and **S. H. Ohb** (2005) Highly efficient overall water splitting through optimization of preparation and operation conditions of layered perovskite photocatalysts. *Topics in Catalysis,* **35,** 3–4.

37. **Kato, H.,** and **A. Kudo** (2001) Water Splitting into H_2 and O_2 on Alkali Tantalate Photocatalysts $ATaO_3$ (A) Li, Na, and K**).** *Journal of Physical Chemistry B***, 105***,* 4285-4292.

38. **Kudo, A.,** and **Y. Miseki,(**2009) Heterogeneous Photocatalyst materials for water splitting. *Chemical Soceity Reviews,* **38**, 253–278.

39. **Liu, Y., B. Huang , Y. Dai, X. Zhang, X. Qin**, and **M. J. M-H Whangbo** (2009) Selective ethanol formation from photocatalytic reduction of carbon dioxide in water with $BiVO_4$ photocatalyst . *Catalysis Communications*, **11,** 210–213

40. **Liua, J.W., G. Chena, Z.H. Lia,** and **Z.G. Zhangb** (2007) Hydrothermal synthesis and Photocatalytic properties of $ATaO_3$ and $ANbO_3$ (A=Na and K). *International Journal of Hydrogen Energy*, **32,** 2269 – 2272.

41. **Li, X.,** and **J. Zang** (2009) Facile Hydrothermal Synthesis of Sodium Tantalate (NaTaO3) Nanocubes and High Photocatalytic Properties. *Journal of Physical Chemistry C* , **113,** 19411–19418.

42. **Luo, D., Y. Bi, W. Kan, N. Zhang**, and **S. Hong,** (2011) Copper and Cerium Co-Doped Titanium dioxide on Catalytic Photo reduction of Carbon dioxide with Water: experimental and theoretical studies. *Journal of Molecular Structure*, doi: 10.1016/j.molstruc.2011.03.044

43. **Liu, B.-J., T. Torimoto,** and **H. Yoneyama,**(1998) Photocatalytic reduction of CO_2 using surface-modified CdS photocatalysts in organic solvent. *Journal of Photochemistry Photobiology A: Chemistry,* **113**, 93-96.

44. **Liu, S., Z. Zhao** and **Z. Wang** (2007) Photocatalytic reduction of carbon dioxide using sol–gel derived titania-supported CoPc catalysts. *Photochemical & Photobiological Sciences*, **6,** 695–700.

45. **Lo, C.C., C. H. Hung, C. S. Yuan,** and **J. F Wu** (2007) Photoreduction of carbon dioxide with H_2 and H_2O over TiO_2 and ZrO_2 in a circulated photocatalytic reactor. *Solar Energy Materials & Solar Cells,* **91**, 1765–1774.

46. **Maginn, E. J, (**2010) What to Do with CO_2 *Journal of Physical Chemistry Letters,* **1**, 3478–3479.

47. **Matthews, R. W.,** and **S. R. McEvoy,** (1992) A comparison of 254 nm and 350 nm excitation of TiO_2 in simple photocatalytic reactors. *Journal of Photochemistry and Photobiology A*: *Chemistry*, **66,** 355–366.

48. **Nam, S. S., H. Kim, G. Kishan, M. J. Choi,** and **K W. Lee**, (1999) Catalytic Conversion of CO_2 to hydrocarbons over rare earth promoted iron catalysts supported on KY Zeolite. *Applied Catalysis A. Gen.,* **179**, 155-159

49. **Patterson, L.,** (1939) The Scherrer Formula for X-Ray Particle Size Determination. Physical Reviews, **56**, 978–982.

50. **Roy, S. C, O. K. Varghese, M. Paulose,** and **C. A. Grimes** (2010) Toward Solar Fuels: Photocatalytic Conversion of Carbon Dioxide to Hydrocarbons. *American Chemical Society Nano letters,* **4,** 1259–1278.

51. **Stroyuk, L., A. I. Kryukov, S. Y. Kuchmii,** and **V. D. Pokhodenko (**2009) Semiconductor Photocatalytic systems for the Production of Hydrogen by the action of visible light**.** *Theoretical and Experimental Chemistry,* **45**, 209-233.

52. **Scibioh, M. A.,** and **B. Viswanathan**, (2004) Electrochemical Reduction of Carbon dioxide: A Status Report. *Proc Indian National Science Academy,* **70**A, 407-462.

53. **Slamet , H. W. Nasution , E. Purnama , S. Kosela,** and **J. Gunlazuardi,**(2005) Photocatalytic reduction of CO_2 on copper-doped Titania catalysts prepared by improved-impregnation method*. Catalysis Communications,* **6**, 313–319.

54. **Shifu. C., Z. Sujuan, L. Wei,** and **Z. Wei,**(2008) Preparation and activity evaluation of p–n junction photocatalyst NiO/TiO_2. *Journal of Hazardous Materials*, **155,** 320–326

55. **Sasirekha, N., Basha, S.J.S.,** and **Shanthi, K.,(**2006) Photocatalytic performance of Ru doped anatase mounted on silica for reduction of carbon dioxide. *Applied Catalysis, B,* **62**, 169–180.

56. **Sayama, K.,** and **H. Arakawa**, (1997) Effect of carbonate salt addition on the photocatalytic decomposition of liquid water over $Pt–TiO_2$ catalyst . *Journal Chemical Society, Faraday T rans.* **93**, 1647-1654.

57. **Seery, M. K., R. George, P. Floris,** and **S. C. Pillai (**2007) Silver doped titanium dioxide nanomaterials for enhanced visible light photocatalysis. *Journal of Photochemistry and Photobiology A: Chemistry,* **189,** 258–263.

58. **Spurr R. A.,** and **H. Myers** (1957), Quantitative Analysis of Anatase-Rutile Mixtures with an X-Ray Diffractometer**.** *Analytical Chem*istry, **29**, 760-761.

59. **Solymosi, F.,** and **I. Tombacz (**1994), Infrared Spectroscopic Study of the Photoinduced Activation of $C0_2$ on $Ti0_2$ and Rb/TiO_2 Catalysts. *Journal of Physical Chemistry,* **98,** 7147-7152.

60. **Tsuneoka, H., K. Teramura, T. Shishido,** and **T. Tanaka** (2010) Adsorbed Species of CO_2 and H_2 on Ga_2O_3 for the Photocatalytic Reduction of CO_2 *Journal of Physical Chemistry C***, 114**, 8892–8898.

61. **Teramura, K., S-i Okuokab, H. Tsuneokab, T. Shishidob,** and **T. Tanaka** (2010) Photocatalytic reduction of CO_2 using H_2 as reductant over $ATaO_3$ photocatalysts (A = Li, Na, K). *Applied Catalysis B: Environmental*, **96**, 565–568.

62. **Tan, S. S., L. Zou,** and **E. Hu**,(2006) Photocatalytic reduction of carbon dioxide into gaseous hydrocarbon using TiO_2 pellets. *Catalysis Today,* **115**, 269–273.

63. **Tseng, I-H., W. C. Chang,** and **J.C.S. Wu** (2002) Photoreduction of CO_2 using sol–gel derived titania and titania-supported copper catalysts. *Applied Catalysis B: Environmental*, **37,** 37–48.

64. **Usubharatana, P., D. McMartin, A. Veawab,** and **P. Tontiwachwuthikul** *Ind*. (2006) Photocatalytic Process for CO_2 Emission Reduction from Industrial Flue Gas Streams. *Eng. Chem. Res***, 45***,* 2558-2568.

65. **Ulagappan, N.,** and **H. Frei**,(2000) Mechanistic Study of CO_2 Photoreduction in Ti Silicalite Molecular Sieve by FT-IR Spectroscopy. *Journal of Physical Chemistry A*, **104,** 7834–7839.

66. **Vargheese, O.K, M.Paulose** and **T. J. Latempa**,(2009) High-Rate Solar Photocatalytic Conversion of CO_2 and Water Vapor to Hydrocarbon Fuels. *Nanoletters*, **9,** 731-737.

67. **Wu,J.C.S.,**and **C.W.Huang,** (2010) In situ DRIFTS study of photocatalytic CO_2 reduction under UV irradiation. *Front.Chem.Eng.China* ,**4,**121-126

68. **Wu, J. C. S., T.-H. Wu, T. Chu, H. Huang,** and **D. Tsai,** (2008) Application of Optical-Fiber Photoreactor for CO_2 Photocatalytic Reduction. *Topic in Catalysis,* **47,** 131–136.

69. **Watanabe, M.,** (1992) Photosynthesis of methanol and methane from CO_2 and H_2O molecules on a ZnO surface. *Surface Science Letters*, **279,** 236-242.

70. **Wang, Y., Y. Wang**, and **Y. Gao** (2010) Photocatalytic H_2 evolution from water in the presence of Carbon dioxide over $NiO/Ca_2Fe_2O_5$ *Reaction Kinetics Mechanics Catalysis*, **99,** 485–491.

71. **Xia X-H ., Z-J. Jia, Y. Yu, Y. Liang, Z. Wang**, and **L-L. Ma,** (2007) Preparation of multi-walled carbon nanotube supported TiO_2 and its Photocatalytic activity in the reduction of CO_2 with H_2O. *Carbon,* **45,** 717–721.

72. **Yan, S C., S. X. Ouyang, J. Gao, M. Yang, J. Y. Feng, X. X. Fan, L. J. Wan, Z. S. Li, J. H. Ye, Y. Zhou**, and **Z. G. Zou (**2010) A Room-Temperature Reactive - Template Route to Mesoporous $ZnGa_2O_4$ with Improved Photocatalytic Activity in Reduction of CO_2. *Angew. Chem. Int. Ed.*, **49,** 6400 – 6404.

73. **Zhang Q.H., W.D.Han, Y.J.Hong** and **J.G.Yu,**(2009) Photocatalytic reduction of CO_2 with H_2O on Pt-loaded TiO_2 catalyst. *Catalysis Today,* **148**, 335-340.